Fisheries and Oceans Canada | Pêches et Océans Canada
Ecosystems and Oceans Science | Sciences des écosystèmes et des océans

Canadian Science Advisory Secretariat (CSAS)

Research Document 2024/040

Quebec Region

End-of-Century Projections of *Calanus* Species Biomass in the Gulf of St. Lawrence, Southern Newfoundland, Scotian Shelf and Northeast Gulf of Maine

Caroline Lehoux[1], Diane Lavoie[1], Catherine L. Johnson[2], Stephane Plourde[1]

[1] Maurice-Lamontagne Institute
Fisheries and Oceans Canada,
850 Route de la Mer,
Mont-Joli, Quebec Canada G5H 3Z4

[2] Bedford Institute of Oceanography
Fisheries and Oceans Canada
PO Box 1006
Dartmouth, Nova Scotia Canada B2Y 4A2

August 2024

Canada

Foreword

This series documents the scientific basis for the evaluation of aquatic resources and ecosystems in Canada. As such, it addresses the issues of the day in the time frames required and the documents it contains are not intended as definitive statements on the subjects addressed but rather as progress reports on ongoing investigations.

Published by:

Fisheries and Oceans Canada
Canadian Science Advisory Secretariat
200 Kent Street
Ottawa ON K1A 0E6

http://www.dfo-mpo.gc.ca/csas-sccs/
csas-sccs@dfo-mpo.gc.ca

ISSN 1919-5044
ISBN 978-0-660-72877-3 Cat. No. Fs70-5/2024-040E-PDF

Correct citation for this publication:

Lehoux, C., Lavoie, D., Johnson, C. L., Plourde, S. 2024. End-of-Century Projections of *Calanus* Species Biomass in the Gulf of St. Lawrence, Southern Newfoundland, Scotian Shelf and Northeast Gulf of Maine. DFO Can. Sci. Advis. Sec. Res. Doc. 2024/040. iv + 53 p.

Aussi disponible en français :

Lehoux, C., Lavoie, D., Johnson, C. L., Plourde, S. 2024. Prédiction de la biomasse des espèces de Calanus *jusqu'à la fin du siècle dans le golfe du Saint-Laurent, au sud de Terre-Neuve, sur le plateau Néo-Écossais et dans le nord-est du golfe du Maine. Secr. can. des avis sci. du MPO. Doc. de rech. 2024/040. iv + 55 p.*

TABLE OF CONTENTS

ABSTRACT

The goal of this study was to describe the potential trajectory of *Calanus* species total biomass in response to future environmental conditions in eastern Canadian waters toward to the end of the 21st century. This was accomplished by using an approach combining Species Distribution Models (SDMs) and regional climate ocean simulations based on the Representative Concentration Pathway 8.5 scenario to project interdecadal abundance and individual body weight. We first built SDMs of *C. finmarchicus*, *C. glacialis* and *C. hyperboreus* with data from the Gulf of Maine to the Gulf of St. Lawrence using covariates extracted from three simulations of a regional climate ocean model driven with downscaled forcing from different Earth System Models. These SDMs were then used to perform past and future decadal projections of abundance and their associated uncertainty among the three regional climate ocean simulations. These abundance projections were then combined with those of individual body weight to describe the interdecadal changes in total *Calanus* biomass. Our SDMs performed similarly well among the three regional climate scenarios. While greater uncertainty was associated with the end of the projection period, total *Calanus* biomass was predicted to decrease toward the end of the century across Canadian waters. However, marked regional differences were noted in amplitude due to varying interplay between local environmental conditions, *Calanus* species composition and individual body weight. In the Fundy-northeast Gulf of Maine and western Scotian Shelf regions in the south, a 60% decrease in total *Calanus* biomass was predicted in 2080-2089 relative to 2000-2009 and was solely driven by a decrease in *C. finmarchicus* abundance and individual body weight. This sharp decrease thus indicated that environmental conditions in these regions would become unfavorable for this species in the future. In the Gulf of St. Lawrence, a 40% decrease in *C. hyperboreus* biomass was partly compensated by a small increase in *C. finmarchicus* biomass, resulting in a 25% decrease in total *Calanus* biomass over the same period, indicating that environmental conditions in this colder region would gradually become less and more favourable to *C. hyperboreus* and *C. finmarchicus* respectively. The decrease in total *Calanus* biomass in the southern Newfoundland region was similar (25%) to the Gulf of St. Lawrence, whereas the decrease forecasted in eastern Scotian Shelf was intermediate (35%) between the southern and northern regions. Assuming that no drastic changes in the ocean circulation occur during the 21st century, our long-term projections suggested that North Atlantic Right Whales (NARW) foraging conditions in the Fundy - northeast Gulf of Maine and western Scotian Shelf will continue to deteriorate at a rate greater than in more northern regions. These predicted patterns of change in future foraging conditions could therefore reinforce the pattern in NARW habitat use and distribution observed since 2010.

1. INTRODUCTION

Calanus spp. are lipid-rich copepods dominating the zooplankton biomass in Canadian waters with region-specific differences in their contribution (Sorochan et al. 2019). Due to their dominance and high biomass, they likely are the preferred preys of North Atlantic Right Whales (NARW, see Table 1 for a complete list of acronyms) in USA and Canadian waters with their availability having an impact on the reproductive success of the population (Meyer-Gutbrod et al. 2015, Baumgartner et al. 2017, Lehoux et al. 2020). In the early 2010s, NARW largely decreased their occupation of traditionally-used foraging habitats in the Great South Channel (spring), Grand Manan and Roseway basin (summer-fall) in response to a decrease in *C. finmarchicus* availability associated with changes in environmental conditions (Record et al. 2019, Sorochan et al. 2019, Meyer-Gutbrod et al. 2023). About one third of the NARW population uses the southern Gulf of St. Lawrence (GSL) since the late 2010s likely because of the combined high abundance of *C. hyperboreus* and relatively shallow bathymetry in the region (Simard et al. 2019, Plourde et al. 2019, Lehoux et al. 2020, Crowe et al. 2021). This recent change in NARW distribution and foraging habitat occupation in response to ocean warming highlighted the need to know how their preferred preys would respond to future climate change in order to adapt the management of NARW in Canadian waters.

Few studies addressed the impact of past and future climate change on the abundance of *Calanus* species in the northwest Atlantic or in Canadian waters. Some studies used surface-only *Calanus* data or highly heterogeneous historical *C. finmarchicus* abundance data collected since the 1950's across the North Atlantic, limiting their analyses to past and future projections of occurrence probability at coarse spatial resolutions inadequate to inform management of NARW in Canadian waters (Reygondeau and Beaugrand 2011, Chust et al. 2014, Villarino et al. 2015). More recently, Grieve et al. (2017) built a Species Distribution Model (SDM) for *C. finmarchicus* using zooplankton data and several regional physical models and predicted a decrease of up to 50% in the abundance of *C. finmarchicus* in the central and northeast Gulf of Maine by the end of the present century. However, no projections were made elsewhere in Canadian waters. Therefore, there are limited information available in the scientific literature to inform about potential changes in *Calanus* prey availability and NARW foraging habitat in Canadian waters.

The goal of this study was to describe the potential trajectory of Calanus species total biomass in response to climate change and environmental conditions expected in eastern Canadian waters by the end of the 21st century. We used different modelling tools to develop an approach including the following elements: (1) Species Distribution Models (SDMs) of C. finmarchicus, C. glacialis and C. hyperboreus abundance, (2) three different regional climate ocean simulations based on the Representative Concentration Pathway 8.5 (RCP 8.5) scenario (Moss et al. 2010) to perform decadal projections of Calanus species abundance and individual body weight, and (3) a combination of these three projections to describe Calanus species assemblage biomass trajectory over the present century. We first adapted a Calanus species SDMs previously described (see Plourde et al. 2024) to the spatial domain and covariates extracted from the three regional climate simulations. We then used these SDMs and the three different regional climate ocean simulations to project Calanus abundance and individual body weight in the future while accounting for the uncertainty in future climate change simulations. These long-term projections provided a strategic information regarding the probable trends in Calanus species assemblage biomass and potential NARW foraging habitat quality in eastern Canadian waters to the end of the century.

2. MATERIAL AND METHODS

2.1. *CALANUS* ABUNDANCE DATA

We used a subset of the dataset used by Plourde et al. (2024) in order to adapt their SDMs to the spatial domain of the regional climate ocean model and simulations used in our study (Lavoie et al. 2020, Lavoie et al. 2021). We used zooplankton data collected by the Atlantic Zone Monitoring Program (AZMP) conducted by the Department of Fisheries and Oceans Canada (DFO) on the Scotian Shelf (SS), in the Gulf of St. Lawrence (GSL) and off southern Newfoundland (sNL) and by the Ecosystem Monitoring (EcoMon) conducted by the National Oceanic and Atmospheric Administration (NOAA) in the Gulf of Maine (GOM) and the part of the Southern New England Shelf (SNE) (Figure 1, left panel). We selected stages CIV, CV and CVI for each species, as these stages were consistently sampled using both the EcoMon 333 µm-mesh nets and the AZMP 200 µm-mesh nets.

EcoMon samples zooplankton up to a depth of 200 m. We applied the method previously described to estimate the unsampled abundance of *C. finmarchicus* and *C. hyperboreus* in the 200-bottom layer (Plourde et al. 2019, Sorochan et al. 2019, Plourde et al. 2024). AZMP stations with bottom depths > 1000 m were excluded from our analyses because areas beyond a bathymetry of 800 m are not sampled as part of the EcoMon surveys. Therefore, 10,431 stations were retained across the transboundary area. Details on sampling efforts are presented Figure A.1.1 in Plourde et al. (2024).

2.2. ENVIRONMENTAL DATA AND COVARIATES

We extracted environmental covariates from a regional climate model simulating ocean environmental conditions between 1971 and 2099 (Lavoie et al. 2021). This ocean circulation model, to which a thermodynamic-dynamic sea-ice model, Louvain-la-Neuve Sea Ice Model (LIM2; Madec et al. 1998) is coupled, is based on the Nucleus for European Modelling of the Ocean (NEMO) system (see details in Brickman and Drozdowski 2012). The modelling system is based on the Océan Parallélisé code, version 9.0 (OPA; Madec 2012) that was applied in Canadian waters (CANOPA). The model covers the GSL, the Scotian Shelf, and the Gulf of Maine with a horizontal grid resolution of 1/12 in latitude and longitude and 46 layers of variable thickness (from 6 m close to the surface to 250 m at near the seafloor). It is a prognostic model, i.e. the temperature and salinity fields are free to evolve with time, and are only constrained through open boundary conditions, freshwater runoff, and surface forcing. The Brickman and Drozdowski (2012) monthly climatologies of temperature and salinity are used to initialize the model and set the open boundary conditions. Tidal components (M2, S2, N2, O1, and K1) are included in the model through surface elevation and barotropic transport at the open boundaries. Freshwater enters the domain through precipitation and runoff from the 78 main rivers. The monthly runoff of the St. Lawrence River is estimated from sea level measurements at Quebec City while runoff for all other rivers is obtained from a hydrological model, providing realistic runoff seasonal patterns (i.e., following precipitation and evaporation). Lavoie et al. (2021) used three-hourly surface forcing data (air temperature, relative humidity, winds, cloud cover, and precipitation) obtained from the Canadian Meteorological Centre - Global Environmental Multiscale (CMC-GEM) atmospheric model (Pellerin et al. 2003) to force the ice–ocean model.

The regional climate model was forced with downscaled atmosphere from three Earth System Models (CanESM2, MPI-ESM-LR, and HadGEM-ES referred to the three simulations onward) using the RCP 8.5. This scenario is considered as the most realistic based on current CO_2 emission levels and using the Earth System Model outputs made available in 2013 through the Coupled Model Intercomparison Project Phase 5 (CMIP5) archive (Schwalm et al. 2020).

The selection of covariates was hypothesis driven, i.e., implying a direct causal mechanistic link between temperature-related covariates and *Calanus* abundance (for more details see Plourde et al. 2024). Briefly, we used the mean temperature in the 0-50 m layer (T_0-50) and the temperature minimum in the water column (Tmin) as proxies of the thermal habitat during active growth and overwintering phases of the *Calanus* life cycle respectively. Bathymetry was included as a proxy for the availability of the different habitats necessary for different parts of their life cycle (Albouy-Boyer et al. 2016, Grieve et al. 2017, Ross et al. 2023) and was extracted from the NOAA database using the marmap R package (NOAA 2022, Pante et al. 2023). Coarse spatial and seasonal patterns in connectivity were considered by applying a formulation based on the '*Availability, supply, and aggregation*' framework (Sorochan et al. 2021. Johnson et al. in preparation[1]) with an emphasis on the elements associated with '*supply*'. Latitude was used as a proxy of the distance from a source region (*Regional population levels*), a spatial climatology of salinity in the 0-50 m layer (climS_0-50sqrt) representing pathways of connectivity along fresher (inner shelf) and saltier (outer shelf) water masses from different source regions (*Advective supply*), and Month to account for species-specific seasonality. Our SDMs did not account for highly dynamic aggregation processes occurring at small spatial scales or highly resolved current dynamics. Spatial climatologies of covariates are presented in Figure 2.

2.3. GENERALIZED ADDITIVE MIXED MODELS

The spatial domain of the present study was larger than previous SDMs based on AZMP data (see Albouy-Boyer et al. 2016) but smaller than more recent SDMs encompassing the northeast USA and Canada shelves from Cape Hatteras to the Labrador Shelf (Plourde et al. 2024). We used Generalized Additive Mixed Models (GAMMs) with monthly averaged regional models covariates associated with each zooplankton value (year, month, latitude, longitude). GAMMs were built for each species and each regional climate model simulation. Our GAMMs followed the general formula:

$$\text{Logit}(\pi_i) \text{ or } \log(\mu_i) = \text{Region} + ti(\text{Month} \times \text{latitude} \times \text{climS\_0\_50sqrt}) + s(\text{T\_0\_50}) + s(\text{Tmin}) + s(\text{log10bathymetry}) + f\text{Year}$$

π_i is the probability of presence for observation i and has a Bernoulli error distribution, μ_i is the abundance given presence and has a Gamma error distribution. The zero-altered Gamma (ZAG) error structure is thus generated by running the GAMM twice (presence/absences; Abundance>0) and combining predictions. Year was used as a random intercept. *s* was a thin plate regression spline (Wood et al. 2003) and *ti* was a tensor product interaction for which we included the main effects and the lower-level interactions (Wood et al. 2006). Our GAMMs considered three regions used as an intercept to account for strong local effect of advection on *Calanus* abundance not considered in the GAMMs formulation, i.e., Cape Cod Bay (CCB), Georges Bank (GB), southern GSL (sGSL), in addition to a large transboundary region encompassing the rest of the study area where key environmental processes are occurring at relatively large scales (Continental Shelf, Figure 1, see Plourde et al. 2024). The dimension of the basis used to represent the smooth term (k) was reduced to avoid overfitting (Tmin <= 8, T_0-50 <=5, bathymetry <=5, month, latitude and climS_0-50sqrt <= 6 for main effect and climS_0-50sqrt <=3 for the interaction).

[1] Johnson, C.L., Plourde, S., Brennan, C.E., Helenius, L.K., Le Corre, N. and Sorochan, K.A. In preparation. The Southern Gulf of St. Lawrence as Foraging Habitat for the North Atlantic Right Whale. DFO Can. Sci. Advis. Sec. Res. Doc.

Plourde et al. (2024) reported an unexpected positive effects on abundance of high temperatures that would be expected to have a negative effect based on species-specific physiological temperature optimums, a pattern that was likely due to the southward transport of *Calanus*. To avoid spurious extrapolation when performing projections at higher temperatures in the future, we winsorized T_0-50 and Tmin at the highest values included in the GAMMs, i.e., the effects and confidence intervals were not allowed to change further than they were at the highest temperature included in the GAMMs (Dixon 1960). The maximum T_0-50 and Tmin were defined separately for the Bernoulli and Gamma GAMMs with each regional model simulation. The percentage of predictions Winsorized was small but was twice as much toward the end of the century as in the reference period (see Table A.2.1).

GAMMs were fitted using the package mgcv (Wood 2017) in R. We used the modified thin plate regression spline that allows the whole term to be shrunk to zero ("ts", Wood 2003). This was not implemented in Plourde et al. (2024) because all terms were highly significant. The smaller spatial domain resulted in some GAMMs that exhibited non-significant relationships with temperature in the Bernoulli GAMM. This type of smoother does covariate selection and avoids using non-significant positive relationships with temperature in projections.

We used a subset of metrics to evaluate SDMs (see Plourde et al. 2024 for details). Bernoulli GAMMs were validated with the True Skill Statistics (TSS) with 30% of data resampled 100 times and with re-substitution. Gamma GAMMs were validated using out of sample deviance on 30% of the data and deviance explained on 100% of the data. The combined predictions $\mu \times \pi$ were validated against observations using the Spearman's correlation coefficient. Homogeneity of residuals and accuracy of predictions were verified graphically. The accuracy of predictions was further assessed with quantile 50, 75, 85, 95% of 10,000 simulations of the Bernoulli and Gamma distribution. Finally, model's robustness was evaluated by performing temporal cross validations. Bernoulli and Gamma GAMMs for the three *Calanus* species and three simulations were first fitted to different blocks of years spanning the 1999-2020 period. Then, models' performance was assessed using the TSS and the Spearman's correlation coefficient between predictions and observations during blocks of years not included to fit the models.

2.4. *CALANUS* PROJECTIONS

2.4.1. Abundance

Projections were performed using monthly decadal climatologies for each regional climate simulation separately. Results were presented as averaged projections of the three simulations for April-October during each decade. Variations among the three regional climate simulations were computed to represent the uncertainty in projected decadal trajectories of various *Calanus*-related metrics (abundance, individual body size, water column biomass). Projections results were reported for each region described in Figure 1 (right panel).

Abundance was projected using the GAMMs without f(Year) (i.e., for an averaged year during the 1999-2020 period).

We estimated the uncertainty in abundance predictions using a simulation-based approach (Miller et al. 2022, Plourde et al. 2024). For each species, GAMMs parameters were simulated 1000 times using the Metropolis Hastings sampler available in the mgcv package (Wood 2017). From the original GAMMs, we extracted the linear predictor matrix (lpmatrix) and spatial grids of the monthly reference climatology used in the projections (2000-2009) for each regional climate simulations. We obtained the expected response ($\pi \times \mu$) for each cell of the prediction grid by the multiplication of the lpmatrix and the simulated parameters. The multiplication of π and μ assumed that they were independent (no covariance). For each cell, the 1000 simulations were

aggregated by month and decade. Therefore, the reported coefficients of variation of predicted abundance for each month, decade, species and position include both the GAMMs parameter uncertainty and the uncertainty of the regional climate simulations.

2.4.2. Individual body weight

Individual body weight (dry weight, mg) was estimated following Plourde et al. (2024). Briefly, we considered T_0-50 during the period of high abundance of CIV during which body size in late stages is determined: May to August for *C. finmarchicus*, and May and June for *C. hyperboreus* and *C. glacialis*. We first estimated the carbon weight of *C. finmarchicus* stages CIV, CV, and CVI in both periods using equations of Campbell et al. (2001). In absence of similar studies for the other two species, we applied scaling factors of 1.6-2.5 and 5-8 to determine the stage-specific body carbon weight of *C. glacialis* and *C. hyperboreus* respectively (Plourde et al. 2019, Helenius et al. 2023). We then converted carbon weight into total individual weight (IDW) assuming that carbon represented on average 52% of body weight for *C. finmarchicus* and *C. glacialis* and 60% for *C. hyperboreus* (Runge et al. 2006, Brey et al. 2010, Helenius et al. 2023). In order to avoid estimating unrealistic body weight at extremely high or low temperature, estimated body weight were constrained to not exceed the lower 10% and upper 90% quantiles of field observations (Helenius et al. 2023).

2.4.3. Water column *Calanus* biomass

In each region (Figure 1, right panel), we estimated total *Calanus* water column biomass in different months and decades as followed:

Biomass (g m^{-2}) = abundance (ind m^{-2}) * IDW (mg) /1000

where IDW was weighted for monthly and regional variations in stage composition (%) using the monthly regional stage proportion of CIV-CVI observed for each species during 1999-2020 (see Figure A.2. 1. in Plourde et al. 2024).

Using 2000-2009 as a reference, we computed past and future interdecadal relative changes (%) in total *Calanus* predicted biomass to describe patterns of significant change in each region. Changes were deemed significant when differences in total *Calanus* water column biomass exceeded 1.96 times the standard deviations (approximation of 95% confidence intervals) between the three sets of predictions obtained with the three regional model simulations. Differences and standard deviations were calculated by region and decade.

3. RESULTS

3.1. SPECIES DISTRIBUTION MODELS (GAMMS)

All performance metrics (TSS, deviance and correlation) were highly similar among the three GAMMs built with the three regional model simulations for each species (Table 2). The performance metrics were similar with Plourde et al (2024) despite the smaller spatial domain considered in our study. Homogeneity and predictions accuracy were provided for the CanESM2_rcp8.5 simulation (e.g., see Figure A.2.1-4). GAMM residuals were homogeneous in all cases. Like in Plourde et al. (2024), there was a slight overestimation of small values and underestimation of large values common in SDMs. The greatest departure from observations was for *C. hyperboreus* with 95% quantile of observations being underestimated by ~ 5000 ind/m² with the GAMM (Figure A.2.4) compared to ~ 2500 ind/m² in Plourde et al. (2024). Other quantiles showed negligeable deviation from observations. Finally, temporal cross-validation using GAMMS fitted with only part of the 1999-2020 dataset generally

performed well when predicting abundance during the other years, indicating that our GAMMs were relatively robust (Table A.2.2). Note that the predicting skills for *C. glacialis* were somewhat lower than for *C. finmarchicus* and *C. hyperboreus* (Table A.2.2).

Smoothers of temperature covariates showed the expected species-specific responses (effects) in both the Bernouilli or Gamma GAMMs (Figure 3). The response to temperature was the most consistent for *C. finmarchicus* with positive effects associated with greater T_0-50 and Tmin than in the other two species (Figure 3). In *C. glacialis* and *C. hyperboreus*, at least one of the Bernouilli and Gamma smoothers for Tmin and T_0-50 showed a strong negative effect of temperature on occurrence or abundance (Figure 3). Overall, the combined effect of temperature covariates in the Gamma GAMMs showed a positive effect on *C. finmarchicus* and *C. hyperboreus* abundance centered in the southern and northern half of the domain, respectively, but with a relatively strong seasonal signal (Figure A.2.7).

The connectivity interaction term showed species-specific seasonal and geographical pattern associated with differences in the relationship of these species with Latitude (Figure 4), Month and water masses (ClimS_0-50sqrt, Figure 5, Figure 6). In *C. finmarchicus*, the positive effect was mostly restricted to eSS, wSS, and GOM from April to July, then only in the extreme south of the spatial domain in the Fall (Figure 6). On the contrary, a high positive effect was observed for *C. glacialis* from May to July in the eGSL, wGSL and sGSL, and for *C. hyperboreus* across the GSL and SS regions from May to September (Figure 6). However, the Gamma GAMM exhibited a positive effect of the connectivity interaction term at the southern limit of the spatial domain for *C. glacialis* early in the season. This effect did not translate into high predicted abundance because the Bernoulli GAMM showed a strong negative effect on abundance in the same area (Figure A.2.5).

The uncertainty around abundance predictions (CV expressed as % of predictions) for the three species of *Calanus* was estimated from April to October during the 2000-2009 decade (reference period for past and future projections, see section 3.2.2). Uncertainty was globally higher for *C. glacialis* than for *C. finmarchicus* and *C. hyperboreus* in the south of the model domain, along the continental slope and in the Strait of Belle Isle (i.e., the most northerly part of the model domain) (Figure 7). Patterns of uncertainty were similar for *C. hyperboreus* and *C. glacialis* whereas *C. finmarchicus* predictions showed the lowest level of uncertainty (Figure 7).

3.2. PROJECTIONS

Results were reported for each region described in Figure 1 (right panel). Spatial patterns in relative change of various covariables and Calanus-associated variables were computed for the decade 2080-2089 relative to 2000-2009 in order to avoid potential larger uncertainty at the end of the projection period (1971-2099).

3.2.1. Trends in temperature covariates

T_0-50 and Tmin averaged over April-October showed similar interdecadal trends in all regions but with initial and final absolute values increasing from the south (GB, Fundy-GOM) to the north (wGSL, eGSL) (Figure 8). The difference between T_0-50 and Tmin was larger in the northernmost regions (GSL, sNL, eSS) where Tmin remained low all year while T_0-50 increased due to the seasonal warming, whereas Tmin increased in late summer and fall in southern regions (Figure A.1.1).

Predicted increases in T_0-50 and Tmin between 2000-2009 and 2080-2089 were not spatially uniform. T_0-50 and Tmin predicted in the GSL in 2080-2089 were similar to those in the Fundy-GOM and wSS region in 2000-2009, while those predicted in 2080-2090 in Fundy-GOM, wSS and part of eSS regions somewhat exceeded temperatures observed in Canadian waters

during 2000-2009 (Figure 9). Increases in T_0-50 were greater in Fundy-GOM, in eSS and sNL, and in areas of the sGSL and eGSL (Figure 9). Increases in Tmin were < 2 °C in the western half of wSS, of 4-5 °C at the northeast half of eSS and western half of sNL, and somewhat in between elsewhere in Canadian waters (3-4 °C). Estimates for temperature increases were on average larger than 3 °C across the model domain.

3.2.2. Trends in *Calanus* abundance

Interdecadal trends in predicted abundance varied among species and regions (Figures 10-12). *C. finmarchicus* abundance was predicted to increase over the present century in northern regions (wGSL, eGSL, sGSL, sNL, eSS). In the wSS, abundance is expected to remain stable until 2060-2069 and then to decrease, whereas in Fundy-GOM and GB, abundance is predicted to show a more steady and continuous decrease over time (Figure 10). The uncertainty around predictions was larger during the later part of the century in all regions and overall greater in Fundy-GOM (Figure 10).

In contrast with *C. finmarchicus*, *C. glacialis* and *C. hyperboreus* predicted abundance showed a consistent negative interdecadal trend over the present century in regions where they were abundant (Figures 11-12). In the wGSL and eGSL, the decreasing interdecadal trend appeared to have started during the 2000-2009 and 2010-2019 decades, respectively (Figures 11-12). In these two species, the uncertainty around predictions was more homogenous among decades than for *C. finmarchicus.* Overall, uncertainty about trends in abundance was greater in the eGSL for C. glacialis and in the wGSL in the case of *C. hyperboreus* (Figures 11-12).

3.2.3. Trends in *Calanus* individual dry weight

The model consistently predicted for all *Calanus* species a steady decrease in predicted decadal IDW across regions over the study period (Figure 13). However, the negative trend appeared steeper during the second half of the century, a pattern particularly prominent for *C. hyperboreus* in regions of the GSL (Figure 13). The uncertainty around these predictions was somewhat larger from 2050 onward (Figure 13).

3.2.4. Trends in *Calanus* biomass

C. finmarchicus was the species showing the highest variability in predicted trends of their biomass among regions, with a stable or increasing predicted biomass in regions from the GSL, a stable then decreasing biomass during the first and second half of the century in sNL and eSS (Figure 14). To the contrary, the model predicted a steady decreasing trend for *C. hyperboreus* and *C. glacialis* biomasses across all regions, with a greater amplitude of change predicted for *C. hyperboreus* in wGSL and eGSL (Figure 14).

Interdecadal trends of total *Calanus* biomass in the different regions generally followed those of the locally dominant species (Figure 15). Total *Calanus* predicted biomass showed a steady decline in both the northern (wGSL, eGSL) and southern (wSS, Fundy-GOM, GB) areas, associated with corresponding decrease in the biomass of *C. hyperboreus* and *C. finmarchicus* respectively (Figure 14). Patterns of variations of total Calanus biomass were not as pronounced in the sGSL, sNL and eSS, but generally showed a decrease from 2060 onward (Figure 15).

Total *Calanus* biomass was predicted to be on average slightly higher during 1971-1999 relative to 2000-2009 across Canadian waters. The first significant decrease in total *Calanus* biomass was predicted to occur earlier in the wGSL, eGSL and sNL (2010-2019) than in Fundy-GOM (2020-2029) and wSS and GB (2030-2039). Decreases in total *Calanus* biomass were significant among all decades in the wGSL, eGSL, Fundy-GOM and GB (Figure 16). However,

large interdecadal relative (%) differences were not always significant, particularly during the 2060-2100 period in sNL, eSS, and wSS (Figure 16) as predictions were associated with large uncertainty (Figure 15).

3.2.5. Decrease in *Calanus* biomass: 2000-2009 vs 2080-2089

The relative changes (%) in species-specific predicted abundance, IDW and water column biomass between 2000-2009 and 2080-2089 reflected the trends previously described in different regions (Table 3). While all metrics showed a marked decrease during 2080-2089 relative to 2000-2009 for *C. glacialis* and *C. hyperboreus* across Canadian waters, a more complex interplay between metrics and regions emerged for *C. finmarchicus* (Table 3). Predicted *C. finmarchicus* abundance was 28-38% greater in 2080-2089 relative to 2000-2009 in northern regions (eSS to wGSL), stable between the two periods in on the wSS, and was 24-31% lower in 2080-2089 in Fundy-GOM and GB compared to 2000-2009 (Table 3). When combined with an estimated region-wide 21-33% decrease in IDW, the resulting pattern in water column biomass over the study period showed a 9-11% increase in the wGSL and eGSL, but no change in the sGSL, a 12-31% decrease in sNL and wSS, and a much larger decrease (50-64%) in wSS, Fundy-GOM and GB (Table 3). Overall, total *Calanus* species biomass was predicted to decrease by 50-65% in GB, Fundy-GOM and wSS, by 25 to 35% in eSS, sNL, eGSL and wGSL, and by 11% in the sGSL between 2000-2009 and 2080-2089 (Table 3).

The relative change (%) in total *Calanus* biomass between 2000-2009 and 2080-2089 was not uniform across seasons and within each region. The largest seasonal pattern occurred in GB, Fundy-GOM and wSS where a sharp decrease in *Calanus* biomass was predicted in summer and fall (Figure 17). Elsewhere, the relative change was greater in June in the sGSL and rather constant in other regions (Figure 17). Spatially, the relative change in total *Calanus* biomass was the greatest in the deep channels of the wGSL and eGSL, offshore in the eastern end of sNL, on the outer shelf in eSS and wSS, and toward the northwest end of the Fundy-GOM-GOM (Figure 18). Interestingly, the relative change in total *Calanus* biomass was the smallest in Roseway basin and along a corridor on the inner shelf of wSS, over a large offshore area in eSS, and on the inner part of sNL (Figure 18).

C. finmarchicus contribution (%) to total *Calanus* predicted biomass is expected to increase across the domain in 2080-2089 relative to 2000-2009 (Figure 19). The largest increase is predicted in the wGSL and eGSL, followed by the sGSL and areas located at the boundary of the eSS and sNL regions (Figure 18). Overall, increases in *C. finmarchicus* contribution (%) to total *Calanus* biomass are more a consequence of a decrease in *C. hyperboreus* and *C. glacialis* biomass than an increase in *C. finmarchicus* biomass (Figure 14).

4. DISCUSSION

4.1. SPECIES DISTRIBUTION MODELS (GAMMS)

Our GAMMs built with data from the GOM to the GSL yielded results similar to a previous study performed on a larger area (Plourde et al. 2024). The small differences in GAMMs performance among regional climate model scenarios were expected given the fact they were built with covariates extracted from the same atmosphere-ocean coupled model albeit some variations in forcing among the three scenarios (ex: atmosphere, river runoff, open boundary conditions; Lavoie et al. 2021). The highly similar quality of our GAMMS gives us confidence in the robustness of our predictions.

Our SDMs showed varying responses to T_0-50 and Tmin among *Calanus* species as previously described using similar modelling approaches (Chust et al. 2014, Albouy-Boyer et al.

2016, Plourde et al. 2024). However, there were some departure from the expected relationships in the cold-water species *C. glacialis* and *C. hyperboreus* likely associated with their transport into southern regions and their persistence under unfavourable warm conditions due to their large lipid reserves (Zakardjian et al. 2003, Helenius et al. 2023, Plourde et al. 2024). Other potential causes for these departures from expected temperature effects are discussed below (see Source of uncertainty).

The 'connectivity' term captured realistic coarse patterns of influence of different waters masses across Canadian waters (see Plourde et al. 2024). Our results suggested that *C. finmarchicus* on the wSS were more associated with water masses with higher salinity originating from the outer shelf or slope water (Head et al.1999, Davies et al. 2014). Patterns of connectivity observed for *C. hyperboreus* highlighted the wGSL as the main source for sGSL and SS along a highly connected outflowing circulation system under the main influence of the freshwater outflow from the St. Lawrence River (Sameoto and Herman 1992, Brennan et al. 2021, Le Corre et al. 2023). Finally, patterns of connectivity indicated that *C. glacialis* would be more associated to Labrador Shelf water and transported in the GSL through the Strait of Belle Isle (Plourde et al. 2024).

SDMs are useful tools to infer patterns during periods and in areas where data are sparsely collected. It is highly recommended to perform predictions and inferences at scales within those considered to be well resolved by the models, which are determined by the temporal and spatial characteristics of the input data (Austin et al. 2007, Waldock et al. 2022). Sampling effort in the AZMP is highly uneven, with most effort during spatial surveys performed twice per year on sparsely distributed hydrographic sections and with a few high-frequency sampling stations visited once or twice a month (Figure 1). In the GOM, the EcoMon sampling effort is better distributed but still substantially uneven among months and regions (Figure 1) (Plourde et al. 2024). Based on these characteristics, we determined that predicting *Calanus* species abundance at the monthly scale was within our models' capacity.

Despite the precautious use of our SDMs at the monthly scales, the uncertainty represented as CV% in model parameters was generally higher at the margins of our spatial domain with uncertainty level markedly different between *C. finmarchicus* (lowest) and *C. glacialis* (highest) (Figure 7). Note that these larger relative CVs were associated with very low predicted abundance of *C. glacialis*, i.e., the absolute CV values were lower than in other areas with high predicted abundance. Nevertheless, larger uncertainties in predictions associated with values at the extreme end of the covariates space is a common feature in SDMs, which indicate that predictions in such areas should be interpreted with caution.

4.2. PROJECTIONS

Our study combined predictions of abundance and IDW to estimate changes in biomass of three important *Calanus* species in Canadian waters. Very few studies have predicted future changes of these species, and all of the predictive studies had significant methodological differences (*Calanus* data, spatial domain and resolution, modelled species, response variable- abundance or occurrence, covariates). Reygondeau and Beaugrand (2011) predicted an unrealistic complete disappearance of *C. finmarchicus* from MAB to the Grand Banks off Newfoundland in 2090-2099 using an ecological niche model based on three covariates and built with a blend of various plankton net data collected across the North Atlantic and low spatial resolution projections. Villarino et al. (2015) used surface only (Continuous Plankton Recorder) *Calanus* data and GAMs with a large set of covariates to predict the probability of occurrence of four *Calanus* species in the North Atlantic at low spatial resolution. They obtained results contrasting those obtained for *C. finmarchicus* in Canadian waters by Reygondeau and Beaugrand (2011). In these two studies, *Calanus* SDM were constructed with large-scale ocean climate models at

coarse spatial scales likely inadequate to resolve physical processes on continental shelves, while predictions were also performed with oceans models at the scale of the North Atlantic with low spatial resolution. Using an approach similar to ours but with input data limited to northeast US waters, Grieve et al. (2017) predicted up to a 50% decrease in averaged *C. finmarchicus* abundance by 2081-2100 relative to the refence period 1977-2013 in the central and northeast GOM. In comparison, our study estimated that abundance and IDW of *C. finmarchicus* from the Fundy-GOM region would decrease by 24% and 32%, respectively, between 2000-2009 and 2080-2089, resulting in a decrease in water column biomass of 64% (Table 3). These differences among studies illustrate the impact of the type of data and characteristics of the ocean climate models used to build SDMs and perform predictions. Our results highlight that using both *Calanus* and environmental covariates at the scale of the processes driving the dynamics of the region of interest is of primary importance when building SDMs and make projections in the future.

The causes of the predicted steady negative trends in *Calanus* biomass differed in the north (wGSL, eGSL) and in the south (wSS, Fundy-GOM, GB). In the north, the negative trend in biomass was associated with declining biomass of the dominant cold water species *C. hyperboreus*, a pattern also observed for the less dominant *C. glacialis*. Abundance of *C. finmarchicus* was predicted to increase, but IDW was predicted to decrease, resulting in a stable biomass. In the south, the steady negative trend in *Calanus* biomass was driven by a decrease in abundance and IDW of *C. finmarchicus*. Therefore, our projections suggest that the GSL would gradually become too warm for the arctic *Calanus* species and a slightly better environment for *C. finmarchicus*, whereas the wSS, Fundy-GOM and GB would become too warm for the sub-arctic *C. finmarchicus*.

Our *Calanus* species abundance and biomass projections were performed at the decadal scale and thus provided an approximation of the potential low frequency trends until the end of the 21st century. We adopted this approach because monthly or annual environmental conditions (ex: T_0-50, Tmin) predicted under these future climate scenarios are considered as highly uncertain (Lavoie et al. 2021). However, past record of physical and biological oceanographic conditions in the northwest Atlantic showed variations occurring at sub-decadal scales (annual, 3-5 years), indicating that higher frequency oscillations between highs and lows in *Calanus* abundance and biomass would likely occur and be superimposed over the long-term trends predicted in our study (DFO 2023).

4.3. DECREASE IN *CALANUS* BIOMASS: 2000-2009 VS 2080-2089

The greater relative change (%) in total *Calanus* biomass between 2000-2009 and 2080-2089 predicted in summer-fall in the southern regions (wSS, Fundy-GOM-GOM, GB) could result from temperature-dependent mechanisms causing a disruption in the phenology of *C. finmarchicus* under warmer conditions. For example, the proportion of lipid-rich CV during summer and fall in the outer Bay of Fundy-GOM near Grand Manan, and in the Wilkinson Basin drastically decreased between 2004-2008 and 2012-2016 despite similar abundance levels of early stages earlier in the season. This suggests a change in the efficiency of the development and growth pathways or in survival leading to the production of abundant lipid-rich resting CV targeted by NARW (Record et al. 2019). In general, the production of a smaller overwintering stock following the development of the first generation and of a more prominent second generation is observed under warmer conditions, and in regions outside the core oceanic habitat of *C. finmarchicus*. No such seasonal relative change in total *Calanus* biomass was observed in other regions. However, the large relative decrease in biomass of the cold water species *C. glacialis* and *C. hyperboreus* predicted in the wGSL and eGSL in 2080-2090 relative to 2000-2009 could be reflective of a negative impact of warmer conditions on the energy

balance, individual body size and amount of energy reserves necessary to fuel reproduction and support overwintering in these species (Plourde et al. 2003, Alcaraz et al. 2014).

The small relative change in *Calanus* biomass predicted in Roseway basin in 2080-2089 (Figure 18) was somewhat surprising. This seems to be driven by a more modest predicted increase in Tmin in this areas in 2080-2089 compared to surrounding regions, likely as a result from the southwestward transport of waters with low Tmin originating from the eSS (Figure 9). This pattern emerged from averaging projections made with three regional climate projections, and might be therefore considered as relatively robust as it was likely associated with a positive effect of the connectivity term on *C. hyperboreus* connecting the GSL, eSS (sources regions) to wSS from May to July (Figure 6). However, these results should be interpreted with caution in the context of long-term projections made with ocean circulation models. Oceanographic conditions in Fundy-GOM, Roseway basin and in wSS are highly sensitive to variations in warm slope waters intrusions, a dynamic representing a challenge to simulate in the present and future with physical ocean models due to the difficulty of modeling the off-shelf boundary conditions (Hebert et al. 2023).

4.4. POTENTIAL CONSEQUENCES FOR NARW DISTRIBUTION AND FORAGING HABITATS

Our study aimed at forecasting the future trajectory of *Calanus* biomass in Canadian waters at the regional and decadal scales. Therefore, our projections provide insights about potential future *Calanus* species population abundance and biomass that would be available and supplied to areas where local physical characteristics (bathymetry, currents, etc.) promote the formation of prey aggregations significant to NARW foraging (Sorochan et al. 2021). Regional and decadal variations in *Calanus* abundance have been associated with fluctuations of NARW population calving success in the past (Meyer-Gutbrod et al. 2015, Sorochan et al. 2019), and recent *Calanus* abundance declines are associated with changes in NARW use of traditional foraging habitats and an overall redistribution across US and Canadian waters (Simard et al. 2019, Meyer-Gutbrod et al. 2023). These strong links between *Calanus* prey abundance and key population dynamics characteristics are the product of processes occurring at the individual and local levels, indicating that our projections provide a useful strategic information for the management of this endangered species in the future.

The spatial and seasonal patterns in the relative (%) decline in total *Calanus* biomass predicted in 2080-2089 compared to 2000-2009 in Fundy-GOM, GB and wSS suggests that the summer and fall decreases in abundance of *C. finmarchicus* late stages observed between the 2000's and 2010's from these regions will continue and become even more pronounced in the future (Record et al. 2019, Meyer-Gutbrod et al. 2023). This predicted decline in *Calanus* availability might negatively impact NARW occupancy of these habitats in the future (Ross et al. 2021). Similar declines in *C. finmarchicus* abundance and negative impacts on NARW abundance have been documented in the Bay of Fundy and Roseway basin (wSS) in summer-early fall, and have resulted in a redistribution of NARW in the 2010's (Record et al. 2019, Meyer-Gutbrod et al. 2023). Our results suggest that it is unlikely that future *Calanus* prey abundance and NARW distribution thereof, would revert to patterns observed in the past in these regions.

In the GSL, *C. finmarchicus* and *C. hyperboreus* biomass showed opposite trends toward the end of the century (2080-2089), but resulted in a net reduction in *Calanus* biomass (-25%) due to the dominance of the *C. hyperboreus* decrease (Figure 13). This decrease in biomass would likely impact the availability of *Calanus* in source regions and its supply to the sGSL, likely resulting in generally lower *Calanus* prey availability in areas such as Gaspé and Shediac Valley where large NARW aggregations are observed since 2015 (Simard et al. 2019, Brennan et al. 2021, Le Corre et al. 2023). Our projections would therefore represent a continuity of the

decreasing pattern in *Calanus* biomass and in NARW potential foraging success documented between 2006 and 2017 in the sGSL (Gavrilchuk et al. 2021). *Calanus* supply to the sGSL is more sensitive to upstream population level in summer-fall than in spring (Brennan et al. 2021), indicating a potentially greater impact of the projected *Calanus* declines during those seasons. In summer-fall, *C. finmarchicus* is the dominant component of *Calanus* flux into the sGSL and its seasonally projected trend is negative during summer-fall (Fig. 5). In spring, variability in *Calanus* supply to the sGSL is more dominated by transport pathways of the dominant species *C. hyperboreus.* However, it was beyond the scope of our study to describe future changes in the transport pathways between source regions (wGSL, eGSL) and the sGSL that could also affect *Calanus* prey abundance in the sGSL (Brennan et al. 2021, Le Corre et al. 2023). Overall, our results suggest that it is unlikely that *Calanus* prey abundance and NARW foraging habitat quality would improve toward the end of the 21st century in our study area.

The eastern Newfoundland (eNL) and Labrador Shelf (LAB) regions were not part of the spatial domain considered in the regional climate model simulations used for our projections. However, field observations and contemporaneous and future projections of sea surface temperature (SST) performed with a variety of global and downscaled ocean climate models could be used to infer the potential future trajectories of *Calanus* biomass in these regions. *Calanus* species biomass in eNL and LAB during 1999-2020 were relatively high but lower than in wGSL and eGSL during summer-Fall (Plourde et al. 2024). In general, past, current and future SST in eNL and LAB are lower during spring-summer-fall than in the adjacent GSL and in southern regions (Lavoie et al. 2013, DFO 2023). Moreover, future projections performed with regional ocean model or with the majority of global ocean models and scenarios suggest that SST would either remain stable or only slightly increase during the current century in these regions (Brickman et al. 2016, IPPC 2023). Under these future temperature conditions, predicted *Calanus* species biomass would likely remain stable or show small changes between 2000-2009 and 2080-2089. In the context of the 25% to 64% decrease of *Calanus* biomass projected in 2080-2089 relative to 2000-2009 in the GSL, sNL, SS and in the Fundy-GOM-GOM regions (Table 3), the presumed *Calanus* biomass levels in eNL and LAB in the future could become more suitable for NARW foraging relative to other regions in Canadian waters.

To conclude, our long-term projections suggested that *Calanus* biomass (NARW foraging conditions) in the Fundy-GOM and wSS would continue to deteriorate toward the end of the century at a greater rate than those projected in eSS, GSL and sNL, possibly reinforcing the current pattern in NARW habitat use and in distribution observed since the early 2010's.

4.5. SOURCES OF UNCERTAINTY

Our projections only considered the combined effects of covariates in our SDMs relative to a reference period (2000-2009), with variations in temperature being the agent of changes in the future. Our projections did not consider some level of year-to-year dependence (autocorrelation) of *Calanus* population, i.e. the abundance of reproducing CVI and the production of a new generation during a given year is associated to the resting stock produced during the previous year. This year-to-year dependency of the population abundance could act as a buffer during periods a low occurrence of years with adverse environmental conditions, but as an accelerator of the decrease during periods of sustained adverse environmental conditions. Consequently, our projections of *Calanus* biomass performed with SDMs to the 2080-2089 decade should be considered as minimal estimates and optimistic.

There is an uncertainty in species identification of *C. finmarchicus* and *C. glacialis* due to some degree of overlap in prosome length in Canadian waters and other North Atlantic regions (Parent et al. 2011, Gabrielsen et al. 2012). In regions of large differences in abundance between these species such as in our study, even a relatively small proportions of

misidentification of the dominant species (C. finmarchicus) could result in substantial errors in the abundance estimates of the less abundant one (C. glacialis) (Parent et al. 2011). Consequently, relationships between the arctic/cold water C. glacialis abundance and covariates could have been 'contaminated' by mis-identifying the more sub-arctic C. finmarchicus, resulting in more 'blurry' smoothers in the SDMs predictions for C. glacialis. Mis-identification of C. finmarchicus could therefore have contributed to the generally larger uncertainty observed in C. glacialis SDM and projections relative to C. finmarchicus (Figure 4, Figure 7).

Although the predicted decreasing future trajectory of *Calanus* individual body weight should be considered as robust, using a constant monthly stage composition (%) in different regions in order to apply these individual body weight to estimate water column *Calanus* biomass could represent a source of uncertainty. This is particularly true for cold water species *C. glacialis* and *C. hyperboreus* with multi-year life cycle with resting stages CIV-V-VI in their core habitats but a life cycle closer to the annual one with a resting population dominated by CV at the southern limit of their distribution as for *C. finmarchicus* (Conover 1988). Therefore, it is possible that the future change in individual body weight would be accompanied by a change in the stage composition that was not taken into account in our study.

The necessity of using a coarse stage category CIV-CVI to limit the number of SDMs and simulations may have impacted our SDMs. C. finmarchicus CIV and CVI female are mostly active in surface layer, whereas CV spend most of its life in deep waters as a resting stage. It means that stage-specific abundance was not always 'directly' connected with T_0-50 and T_min. It was not the case for C. hyperboreus and C. glacialis in which CIV-CV-CVI are all resting stages in Canadian waters. The departure of some of the smoothers describing the effect of T_0-50 on C. glacialis and C. hyperboreus from the expected temperature-Calanus relationships could have been associated to this disconnection between abundance and covariates on the vertical dimension.

The projected IDW are within the observed values (Plourde et al. 2019; Sorochan et al. 2019). However, we did not account for effect of food level which could also be a substantial driver of variations in body size (Campbell et al. 2001). The biogeochemical model (Lavoie et al. 2021) included projections of chlorophyll *a* concentration. However, changes in chlorophyll *a* were not significant between their two reference periods (1991-2010 and 2061-2080). Moreover, Campbell et al. (2001) did not test for the temperature*food interaction making it difficult to include both effects in our approach.

Our *Calanus* biomass projections using SDMs were made assuming that no drastic changes in the circulation mode and predicted trends in oceanographic conditions would occur during the 1971-2100 period. However, a change in the Atlantic Meridional Overturning Circulation (AMOC) before the end of the 21st century due to modifications in oceanographic conditions was deemed possible yet highly uncertain (Ditlevsen and Ditlevsen 2023). The impacts of a drastic change in the circulation mode of major features such as the Labrador Current and the Gulf Stream are highly uncertain but could modify currents strength, patterns of connectivity among regions, and local oceanographic conditions and plankton productivity (Lavoie et al. 2021, Rutherford et al. 2024).

5. REFERENCES CITED

Albouy-Boyer, S., Plourde, S., Pepin, P., Johnson, C.L., Lehoux, C., Galbraith, P.S., Hebert, D., Lazin, G., and Lafleur, C. 2016. Habitat modelling of key copepod species in the Northwest Atlantic Ocean based on the Atlantic Zone Monitoring Program. J. Plankton Res. 38: 589–603. Doi:10.1093/plankt/fbw020.

Alcaraz, M., Felipe, J., Grote, U., Arashkevich, E., and Nikishina, A. 2014. Life in a warming ocean: thermal thresholds and metabolic balance of arctic zooplankton. J. Plankton Res. 36: 3-10.

Austin, M. 2007. Species distribution models and ecological theory: a critical assessment and some possible new approaches. Ecol. Model. 200: 1-19.

Baumgartner, M.F., Wenzel, F.W., Lysiak, N.S.J. and Patrician, M.R. 2017. North Atlantic right whale foraging ecology and its role in human-caused mortality. Mar. Ecol. Prog. Ser. 581 : 165−181.

Brennan, C. E., Maps, F., Gentleman, W. C., Lavoie, D., Chassé, J., Plourde, S., and Johnson, C. L. 2021. Ocean circulation changes drive shifts in *Calanus* abundance in North Atlantic right whale foraging habitat: a model comparison of cool and warm year scenarios. Prog. Oceanogr. 197: 102629.

Brickman, D., and Drozdowski, A. 2012. Development and validation of a regional shelf model for Maritime Canada based on the NEMO-OPA circulation model. Can. Tech. Rep. Hydrogr. Ocean Sci. 278: vii + 57.

Brey, T., Müller-Wiegmann, C., Zittier, Z.M.C., and Hagen, W. 2010. Body composition in aquatic organisms - A global data bank of relationships between mass, elemental composition and energy content. J. Sea Res. 64: 334–340.

Brickman, D., Zeliang, W., and DeTracey, B. 2016. High Resolution Future Climate Model Simulations for the Northwest Atlantic. Can. Tech. Rep. Hydrogr. Ocean. Sci. 315: xiv + 143.

Campbell, R.G., Wagner, M.M., Teegarden, G.J., Boudreau, C.A., and Durbin, E.G. 2001. Growth and development rates of the copepod *Calanus finmarchicus* reared in the laboratory. Mar. Ecol. Prog. Ser. 221: 161–183. Doi:10.3354/meps221161.

Chust, G., Castellani, C., Licandro, P., Ibaibarriaga, L., Sagarminaga, Y., and Irigoien, X. 2014. Are *Calanus* spp. Shifting poleward in the North Atlantic? A habitat modelling approach. ICES J. Mar. Sci. 71: 241-253.

Conover, R. J. 1988. Comparative life histories in the genera *Calanus* and Neocalanus in high latitudes of the northern hemisphere. Hydrobiologia, 167: 127-142.

Crowe, L. M., Brown, M. W., Corkeron, P. J., Hamilton, P. K., Ramp, C., Ratelle, S., Vanderlaan, A.S.M. and Cole, T. V. 2021. In plane sight: a mark-recapture analysis of North Atlantic right whales in the Gulf of St. Lawrence. Endanger. Species Res. 46: 227-251.

Davies, K.T., Taggart, C.T., and Smedbol, R.K. 2014. Water mass structure defines the diapausing copepod distribution in a right whale habitat on the Scotian Shelf. Mar. Ecol. Prog. Ser. 497: 69-85.

DFO. 2023. Oceanographic Conditions in the Atlantic Zone in 2022. DFO Can. Sci. Advis. Sec. Sci. Advis. Rep. 2023/019.

Ditlevsen, P., and Ditlevsen, S. 2023. Warning of a forthcoming collapse of the Atlantic meridional overturning circulation. Nat. Commun. 14: 1-12.

Dixon W.J. 1960. Simplified Estimation from Censored Normal Samples. Ann. Math. Stat. 31:385–391.

Gabrielsen, T. M., Merkel, B., Søreide, J. E., Johansson-Karlsson, E., Bailey, A., Vogedes, D., Nygard, H., Varpe, O. and Berge, J. 2012. Potential misidentifications of two climate indicator species of the marine arctic ecosystem: *Calanus glacialis* and *C. finmarchicus*. Polar biol. 35: 1621-1628.

Gavrilchuk, K., Lesage, V., Fortune, S.M.E., Trites, A.W., and Plourde, S. 2021. Foraging habitat of North Atlantic right whales has declined in the Gulf of St. Lawrence, Canada, and may be insufficient for successful reproduction. Endanger. Species Res. 44: 113–136. Doi:10.3354/ESR01097.

Grieve, B. D., Hare, J. A., and Saba, V. S. 2017. Projecting the effects of climate change on *Calanus finmarchicus* distribution within the US Northeast Continental Shelf. Sci. Rep. **7** : 1-12. Doi:10.1038/s41598-017-06524-1.

Head, E. J., Harris, L. R., and Petrie, B. 1999. Distribution of *Calanus* spp. on and around the Nova Scotia Shelf in April: evidence for an offshore source of *Calanus finmarchicus* to the central and western regions. Can. J. Fish. Aquat. Sci. 56: 2463-2476.

Hebert, D., Layton, C., Brickman, D., and Galbraith, P.S. 2023. Physical Oceanographic Conditions on the Scotian Shelf and in the Gulf of Maine during 2022. Can. Tech. Rep. Hydrogr. Ocean Sci. 359: vi + 81 p.

Helenius, L.K., Head, E.J.H., Jekielek, P., Orphanides, C.D., Pepin, P., Perrin, G., Plourde, S., Ringuette, M., Runge, J.A., Walsh, H.J., and Johnson, C.L. 2023. Spatial variability of *Calanus* spp. size and lipid content in the northwest Atlantic – Compilation and brief summary of historical observations, 1977-2020. Can. Tech. Rep. Fish. Aquat. Sci. 3549: iv + 58 p

IPCC. 2023. Summary for Policymakers. In: Climate Change 2023: Synthesis Report. Contribution of Working Groups I, II and III to the Sixth Assessment Report of the Intergovernmental Panel on Climate Change [Core Writing Team, H. Lee and J. Romero (eds.)]. IPCC, Geneva, Switzerland, pp. 1-34, doi: 10.59327/IPCC/AR6-9789291691647.001

Lavoie, D., Lambert, N., Ben Mustapha, S. and van der Baaren, A. 2013. Projections of future physical and biogeochemical conditions in the Northwest Atlantic from CMIP5 Global Climate Models. Can. Tech. Rep. Hydrogr. Ocean Sci. 285: xiv + 156 pp.

Lavoie, D., Lambert, N., Rousseau, S., Dumas, J., Chassé, J., Long, Z., Perrie, W., Starr, M., Brickman, D., and Azetsu-Scott, K. 2020. Projections of future physical and biochemical conditions in the Gulf of St. Lawrence, on the Scotian Shelf and in the Gulf of Maine using a regional climate model. Can. Tech. Rep. Hydrogr. Ocean Sci. 334: xiii + 102

Lavoie, D., Lambert, N., Starr, M., Chassé, J., Riche, O., Le Clainche, Y., Azetsu-Scott, K., Béjaoui, B., Christian, J.R., and Gilbert, D. 2021. The Gulf of St. Lawrence Biogeochemical Model: A Modelling Tool for Fisheries and Ocean Management. Front. Mar. Sci. 8: 1–29. Doi:10.3389/fmars.2021.732269.

Le Corre, N., Brennan, C. E., Chassé, J., Johnson, C. L., Lavoie, D., Paquin, J. P., Soontiens, N. and Plourde, S. 2023. A biophysical model of *Calanus hyperboreus* in the Gulf of St. Lawrence: Interannual variability in phenology and circulation drive the timing and location of right whale foraging habitat in spring and early summer. Progr. Oceanogr. 219: 103152.

Lehoux, C., Plourde S., and Lesage, V. 2020. Significance of dominant zooplankton species to the North Atlantic Right Whale potential foraging habitats in the Gulf of St. Lawrence: a bio-energetic approach. DFO Can. Sci. Advis. Sec. Res. Doc. 2020/033. iv + 44 p.

Madec, G. 2012. NEMO Ocean Engine. Note du Pôle de modélisation, Vol. 27. Guyancourt: de l'Institut Pierre-Simon Laplace.

Madec, G., Delecluse, P., Imbard, M., and Lévy, C. 1998. OPA 8.1 Ocean General Circulation Model reference manual. Note du Pôle de modélisation, Vol. 11. Guyancourt: de l'Institut Pierre-Simon Laplace.

Meyer-Gutbrod, E. L., Greene, C. H., Sullivan, P. J., and Pershing, A. J. 2015. Climate-associated changes in prey availability drive reproductive dynamics of the North Atlantic right whale population. Mar. Ecol. Prog. Ser. 535: 243-258.

Meyer-Gutbrod, E. L., Davies, K. T., Johnson, C. L., Plourde, S., Sorochan, K. A., Kenney, R. D., Ramp, C., Gosselin, J-F, Lawson, J.W. and Greene, C. H. 2023. Redefining North Atlantic right whale habitat-use patterns under climate change. Limnol. Oceanogr. 68**:** S71-S86.

Miller, D. L., Becker, E. A., Forney, K. A., Roberts, J. J., Cañadas, A., and Schick, R. S. 2022. Estimating uncertainty in density surface models. PeerJ, 10: e13950.

Moss, R.H., Edmonds, J.A., Hibbard, K.A., Manning, M.R, Rose,S.K., van Vuuren, D.P., Carter, T.R., Emori, S., Kainuma, M., Kram, T., Meehl, G.A., Mitchell, J.F.B, Nakicenovic, N., Riahi, K., Smith, S.J., Stouffer, R.J., Thomson, A.M., Weyant, J.P. and Wilbanks, T.J. 2010. The next generation of simulations for climate change research and assessment. Nature 463: 747-756.

NOAA National Centers for Environmental Information. 2022. ETOPO 2022 15 Arc-Second Global Relief Model. NOAA National Centers for Environmental Information. doi:doi.org/10.25921/fd45-gt74.

Pante, E., Simon-Bouhet, B., and Irisson, J. 2023. marmap: Import, Plot and Analyze Bathymetric and Topographic Data. R package version 1.0.10.

Parent, G. J., Plourde, S., and Turgeon, J. 2011. Overlapping size ranges of *Calanus* spp. off the Canadian Arctic and Atlantic Coasts: impact on species' abundances. J. Plankton Res. 33: 1654-1665. Doi:10.1093/plankt/fbr072.

Pellerin, G., Lefaivre, L., Houtekamer, P., and Girard, C. 2003. Increasing the horizontal resolution of ensemble forecasts at CMC. Nonlinear Proc. Geoph. 10: 463–468. doi: 10.5194/npg-10-463-2003

Plourde, S., Joly, P., Runge, J. A., Dodson, J., and Zakardjian, B. 2003. Life cycle of *Calanus hyperboreus* in the lower St. Lawrence Estuary and its relationship to local environmental conditions. Mar. Ecol. Prog. Ser. 255: 219-233.

Plourde, S., Lehoux, C., Johnson, C.L., Perrin, G., and Lesage, V. 2019. North Atlantic right whale (*Eubalaena glacialis*) and its food: (I) a spatial climatology of *Calanus* biomass and potential foraging habitats in Canadian waters. J. Plankton Res. 41(5): 667–685. Doi:10.1093/plankt/fbz024.

Plourde, S., Lehoux, C., Roberts, J.J., Johnson, C., Record, N., Pepin, P., Orphanides, C., Schick, R.S., Walsh, H., Ross, C.H. 2024. Describing the Seasonal and Spatial Distribution of *Calanus* Prey and North Atlantic Right Whale Potential Foraging Habitats in Canadian Waters Using Species Distribution Models. DFO Can. Sci. Advis. Sec. Res. Doc. 2024/039. v + 71 p.

Record, N. R., Runge, J. A., Pendleton, D. E., Balch, W. M., Davies, K. T., Pershing, A. J., Catherine L. Johnson, Stamieszkin, K., Ji, R., Feng, Z., Kraus, S.D., Kenney, R.D., Hudak, C.A., Mayo, C.A., Chen, C., Salisbury, J.E. and Thompson, C. R. 2019. Rapid climate-driven circulation changes threaten conservation of endangered North Atlantic right whales. Oceanography 32: 162–169.

Reygondeau, G. and Beaugrand, G. 2011. Future climate-driven shifts in distribution of *Calanus finmarchicus*. Glob. Change Biol. 17: 756-766.

Ross, C.H., Pendleton, D.E., Tupper, B., Brickman, D., Zani, M.A., Mayo, C.A. and Record, N.R. 2021. Projecting regions of North Atlantic right whale, *Eubalaena glacialis*, habitat suitability in the Gulf of Maine for the year 2050. Elem. Sci. Anth., 9: 1.

Ross, C. H., Runge, J. A., Roberts, J. J., Brady, D. C., Tupper, B., and Record, N. R. 2023. Estimating North Atlantic right whale prey based on *Calanus finmarchicus* thresholds. Mar. Ecol. Prog. Ser. 703: 1-16.

Runge, J.A., Plourde, S., Joly, P., Niehoff, B., and Durbin, E. 2006. Characteristics of egg production of the planktonic copepod, *Calanus finmarchicus*, on Georges Bank: 1994-1999. Deep. Res. Part II Top. Stud. Oceanogr. 53: 2618–2631. doi:10.1016/j.dsr2.2006.08.010.

Rutherford, K., Fennel, K., Garcia Suarez, L., and John, J. G. 2024. Uncertainty in the evolution of northwest North Atlantic circulation leads to diverging biogeochemical projections. Biogeosciences, 21, 301–314.

Sameoto, D. D. and Herman, A. W. 1992. Effect of the outflow from the Gulf of St. Lawrence on Nova Scotia shelf zooplankton. Can. J. Fish. Aquat. Sci. 49: 857-869.

Schwalm, C.R., Glendon, S., and Duffy, P.B. 2020. RCP8.5 tracks cumulative CO2 emissions. Proc. Natl. Acad. Sci. U.S.A. 117: 19656–19657. doi:10.1073/PNAS.2007117117.

Simard, Y., Roy, N., Giard, S., and Aulanier, F. 2019. North Atlantic right whale shift to the Gulf of St. Lawrence in 2015, revealed by long-term passive acoustics. End. Species Res. 40: 271-284.

Sorochan, K.A., Plourde, S., Morse, R., Pepin, P., Runge, J., Thompson, C., and Johnson, C.L. 2019. North Atlantic right whale (*Eubalaena glacialis*) and its food: (II) interannual variations in biomass of *Calanus* spp. on western North Atlantic shelves. J. Plankton. Res. 41: 687–708. doi:10.1093/plankt/fbz044.

Sorochan, K.A., Plourde, S., Baumgartner, M.F., and Johnson, C.L. 2021. Availability, supply, and aggregation of prey (*Calanus* spp.) in foraging areas of the North Atlantic right whale (*Eubalaena glacialis*). ICES J. Mar. Sci. 78: 3498–3520. doi:10.1093/icesjms/fsab200.

Villarino, E., Chust, G., Licandro, P., Butenschön, M., Ibaibarriaga, L., Larrañaga, A., and Irigoien, X. 2015. Modelling the future biogeography of North Atlantic zooplankton communities in response to climate change. Mar. Ecol. Prog. Ser. 531: 121–142. Doi:10.3354/meps11299.

Waldock, C., Stuart-Smith, R.D., Albouy, C., Cheung, W.W., Edgar, G.J., Mouillot, D., Tjiputra, J. and Pellissier, L. 2022. A quantitative review of abundance-based species distribution models. Ecography 2022: e05694.

Wood, S.N. 2003. Thin plate regression splines. J. R. Statist. Soc. B. 65:95-114.

Wood, S.N. 2006. Low rank scale invariant tensor product smooths for generalized additive mixed models. Biometrics 62:1025-1036.

Wood, S.N. 2017. Generalized Additive Models: An Introduction with R (2nd edition). Chapman and Hall/CRC.

Zakardjian, B. A., Sheng, J., Runge, J. A., McLaren, I., Plourde, S., Thompson, K. R., and Gratton, Y. 2003. Effects of temperature and circulation on the population dynamics of *Calanus finmarchicus* in the Gulf of St. Lawrence and Scotian Shelf: Study with a coupled, three-dimensional hydrodynamic, stage-based life history model. J. Geophys. Res. (Oceans). 108 (C11).

6. ACKNOWLEDGMENTS

We thank all the DFO and NOAA scientists and crew of the research vessels who contributed to the collection of AZMP and EcoMon zooplankton samples. Special thanks are due to the DFO taxonomists and scientists at the Plankton Sorting and Identification Center of the National Marine Fisheries Research Institute, Poland, for processing AZMP and EcoMon plankton samples respectively. We thank F. Cyr, D. Bélanger and B. Casault for providing AZMP environmental and *Calanus* data, and H.J. Walsh for providing the same data collected by EcoMon. K. Sorochan provided suggestions that contributed to improve the text. S. Plourde, C. Lehoux, C.L. Johnson and D. Lavoie were supported by DFO Science.

7. TABLES

Table 1. List of acronyms

Acronym	Full name
SDMs	Species Distribution Models
NARW	North Atlantic Right Whale
RCP 8.5	Representative Concentration Pathway 8.5
AZMP	Atlantic Zone Monitoring Program
DFO	Department of Fisheries and Oceans Canada
SS	Scotian Shelf
GSL	Gulf of St. Lawrence
sNL	southern Newfoundland
EcoMon	Ecosystem Monitoring Program
NOAA	National Oceanic and Atmospheric Administration
GOM	Gulf of Maine
SNE	Southern New England shelf
CIV	copepodite stage IV
CV	copepodite stage V
CVI	copepodite stage VI
T_0-50	temperature in 0-50 m layer
Tmin	temperature minimum in the water column
climS_0-50sqrt	spatial climatology of salinity in the 0-50 m layer
USA	United States of America
GAMMs	Generalized Additive Mixed Models
CCB	Cape Cod Bay
GB	Georges Bank
sGSL	southern GSL
IDW	individual dry weight
Fundy-GOM	Fundy- gulf of Maine
wGSL	western gulf of St. Lawrence
eGSL	eastern gulf of St. Lawrence
eSS	eastern Scotian Shelf
wSS	western Scotian Shelf
sNL	southern Newfoundland shelf
LAB	Labrador Shelf

Table 2. Results for Bernoulli and Gamma GAMMs by ocean model simulation. The Bernoulli GAMMs were validated across the 100 iterations refitted with 70% of the stations; 30% were used to calculate the TSS (mean ± sd). The TSS was also calculated while resubstiting the 100% of data used to fit the model. The Akaike information criterion (AIC) used for model comparison, and the restricted maximum likelihood are presented for both model distributions. The Gamma GAMMs were validated using out-of-sample deviance on 30% of the data (70% for model fitting) and the deviance explained using resubstitution. The combined predictions of the two models (π x μ) was validated using the Spearman's correlation coefficient. n=10431.

		Bernoulli				Gamma				Combined
Species	Model	TSS (30%)	TSS (100%)	AIC	REML	Out of sample deviance (30%)	Deviance explained (100%)	AIC	REML	Spearman's correlation coefficient
C. finmarchicus	CanESM2_rcp8.5	0.52±0.06	0.63	1188	598	4402	48.0	207409	103844	0.73
	HadGEM2-ES_rcp8.5	0.52±0.05	0.64	1179	597	4438	47.5	207516	103886	0.73
	MPI-ESM-LR_rcp8.5	0.53±0.04	0.64	1180	597	4425	47.6	207502	103905	0.73
C. glacialis	CanESM2_rcp8.5	0.84±0.00	0.85	3369	1753	603	47.2	36404	18299	0.67
	HadGEM2-ES_rcp8.5	0.85±0	0.85	3394	1766	610	46.1	36449	18313	0.68
	MPI-ESM-LR_rcp8.5	0.85±0	0.85	3385	1763	615	46.9	36420	18317	0.67
C. hyperboreus	CanESM2_rcp8.5	0.68±0.01	0.7	7059	3595	1784	59.9	76300	38249	0.77
	HadGEM2-ES_rcp8.5	0.68±0.01	0.69	7074	3603	1831	60.2	76255	38234	0.77
	MPI-ESM-LR_rcp8.5	0.68±0.01	0.69	7081	3606	1871	59.5	76335	38258	0.77

Table 3. Percentage of change of Calanus species abundance (N m^{-2}), individual dry weight (IDW) and biomass (g m^{-2}) between 2080-2089 and 2000-2009. Bold values= increase, negative values = decrease.

	C. finmarchicus			*C. glacialis*			*C. hyperboreus*			*Calanus* spp.
Region	Abundance	IDW	Biomass	Abundance	IDW	Biomass	Abundance	IDW	Biomass	Biomass
wGSL	**29**	-22	**11**	-17	-19	-33	-18	-24	-38	-25
eGSL	**35**	-25	**9**	-22	-23	-45	-21	-25	-42	-26
sGSL	**28**	-25	**1**	-32	-21	-49	-22	-27	-40	-11
sNL	**38**	-33	-12	-36	-28	-55	-28	-19	-44	-25
eSS	**32**	-33	-31	-38	-27	-62	-27	-23	-47	-35
wSS	-2	-29	-61	-42	-25	-64	-26	-25	-48	-60
Fundy-GOM	-24	-32	-64	-61	-29	-75	-30	-34	-54	-64
GB	-31	-21	-50	-55	-24	-54	-25	-27	-15	-49

8. FIGURES

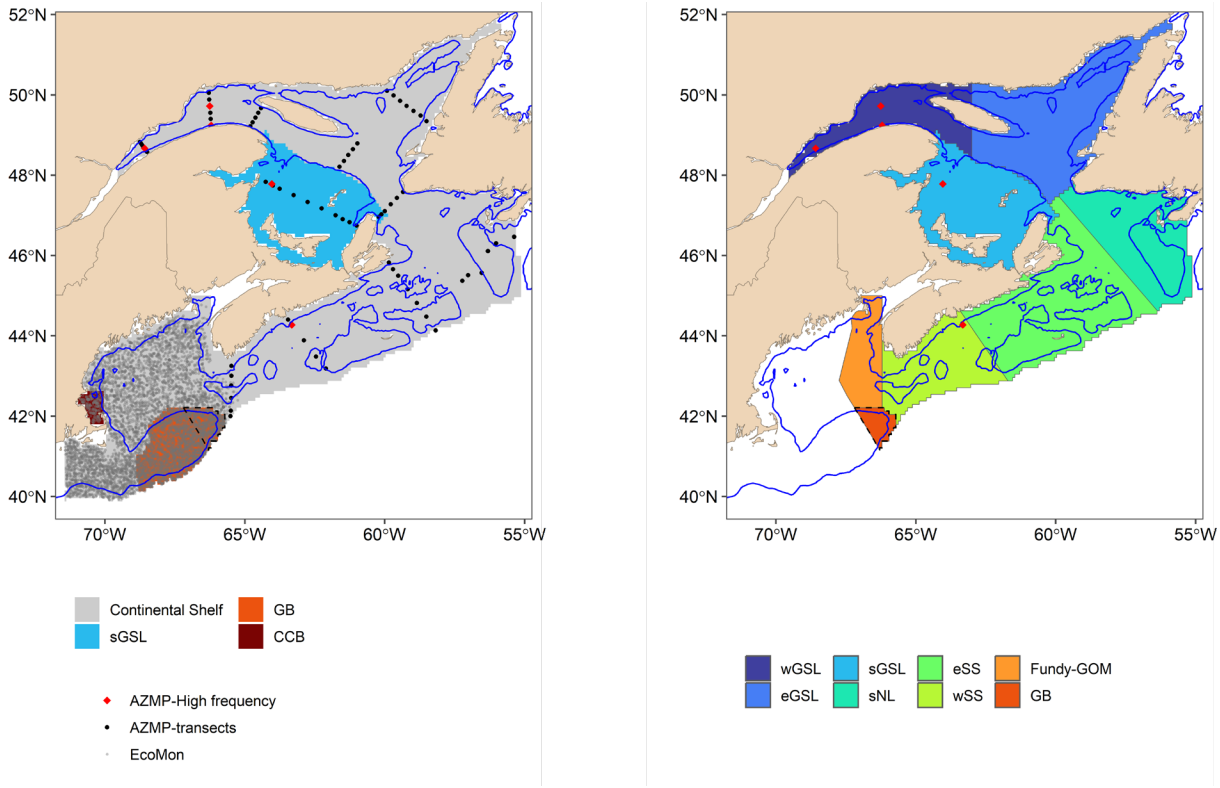

Figure 1. Sampling area of the Atlantic Zone Monitoring Program (AZMP) used in this study. The transects are identified with black dots and high-frequency fixed stations are identified with red square. Blue lines represent the 100-m isobath. The colors in the left panel indicate the regions used in the GAMMs. The colors in the right panel indicate the regions used for reporting results. wGSL: western Gulf of St. Lawrence, eGSL: eastern Gulf of St. Lawrence, sGSL: southern Gulf of St. Lawrence, sNL: southern Newfoundland Labrador, eSS: eastern Scotian Shelf, wSS: western Scotian Shelf, Fundy-GOM: Bay of Fundy-Gulf of Maine, CCB: Cape Cod Bay, GB: Georges Bank. See Figure A.1.2 for other geographic locations mentioned in the document.

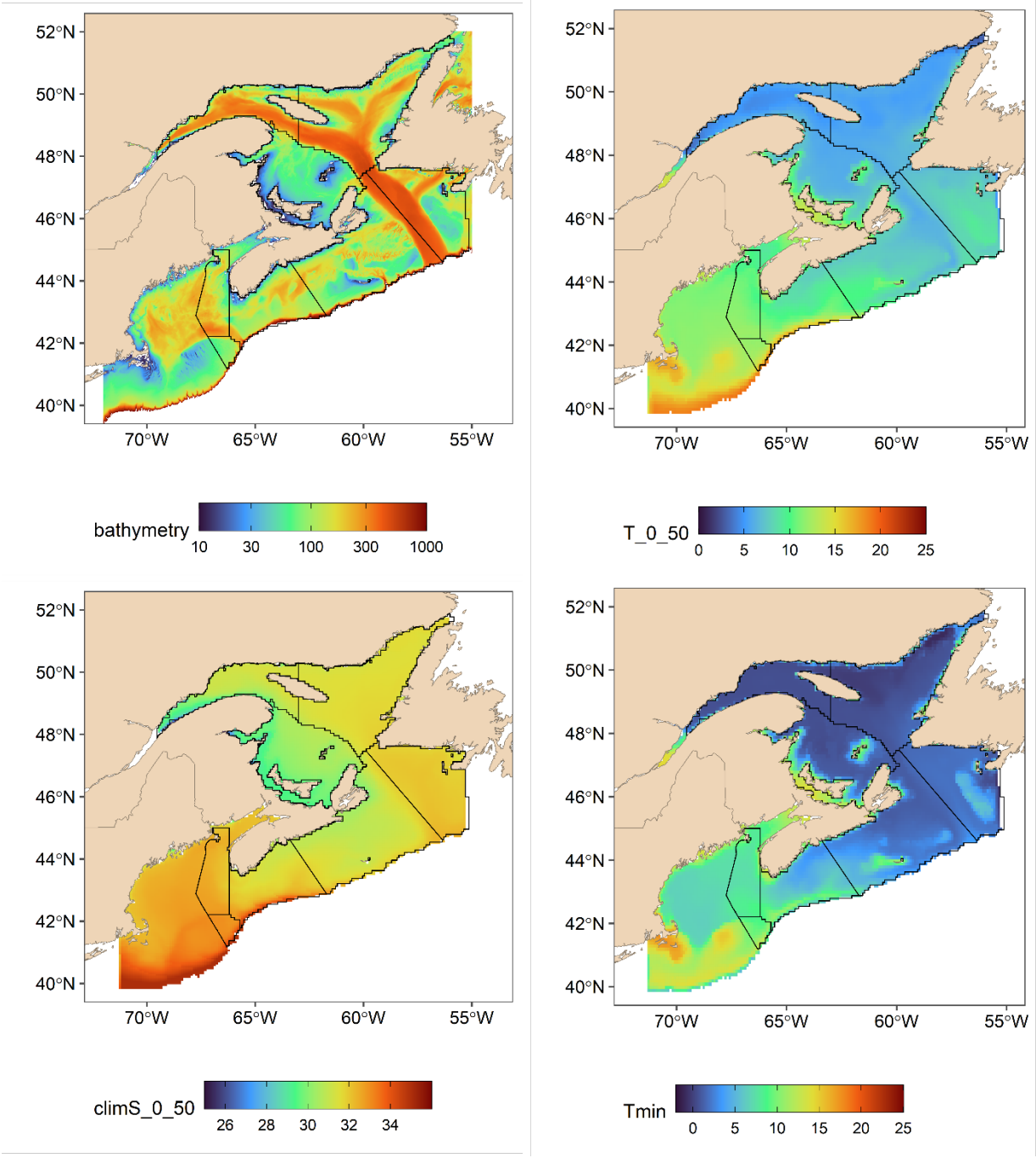

Figure 2. Maps of covariates with a spatial dimension used in GAMMs. Covariates were averaged across three regional climate simulations during 1999-2020 for April-October (T_0-50 and Tmin) and January-December for ClimS_0-50. Black lines represent boundaries of regions used to report results.

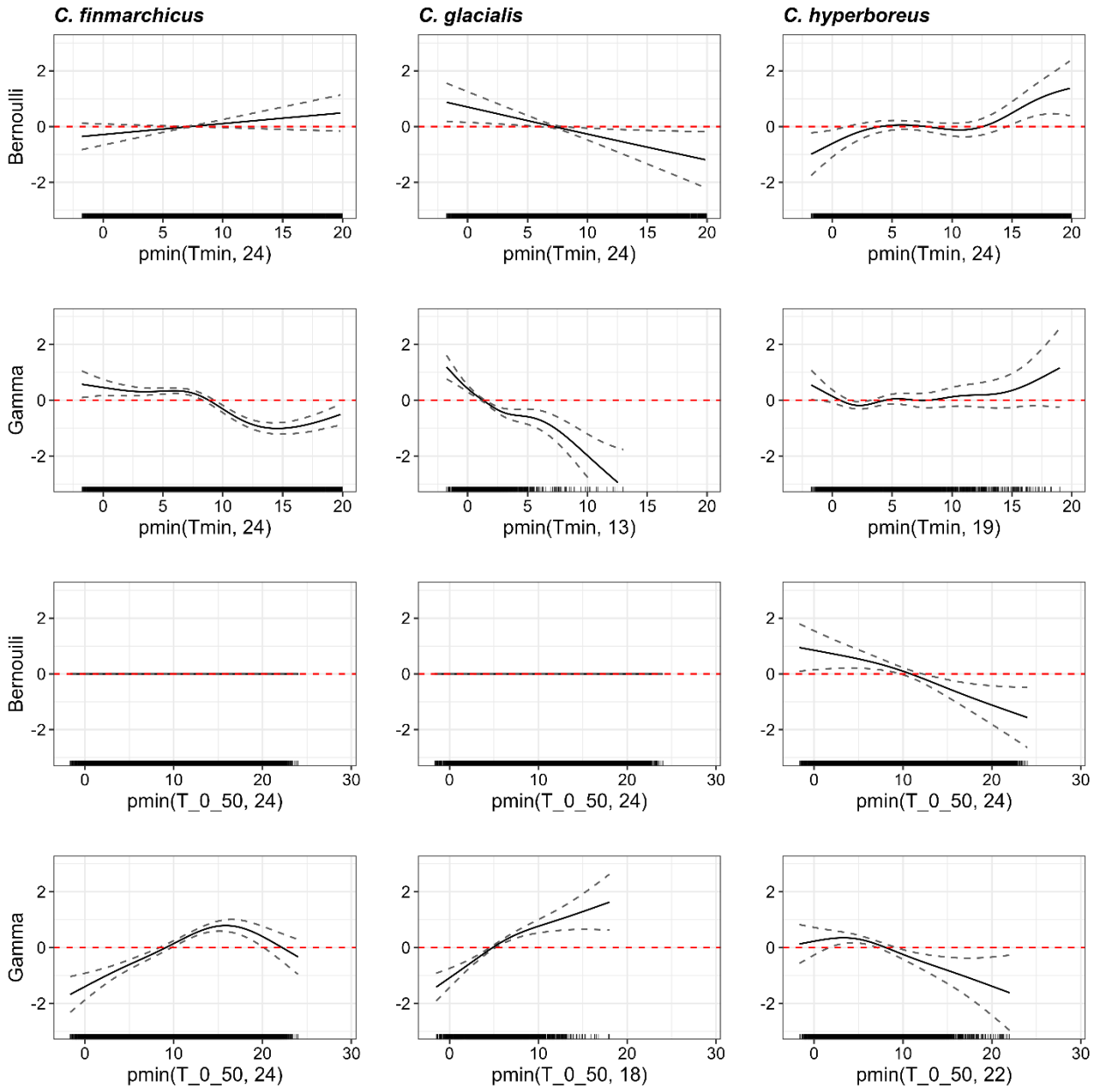

Figure 3. Partial effects for T_0_50 and Tmin of the Bernoulli and Gamma GAMMs for C. finmarchicus*,* C. glacialis*, and* C. hyperboreus *with the CanESM2_rcp8.5 simulation. pmin (covariate, x) indicate Winsorizing of predictions at covariate value x.*

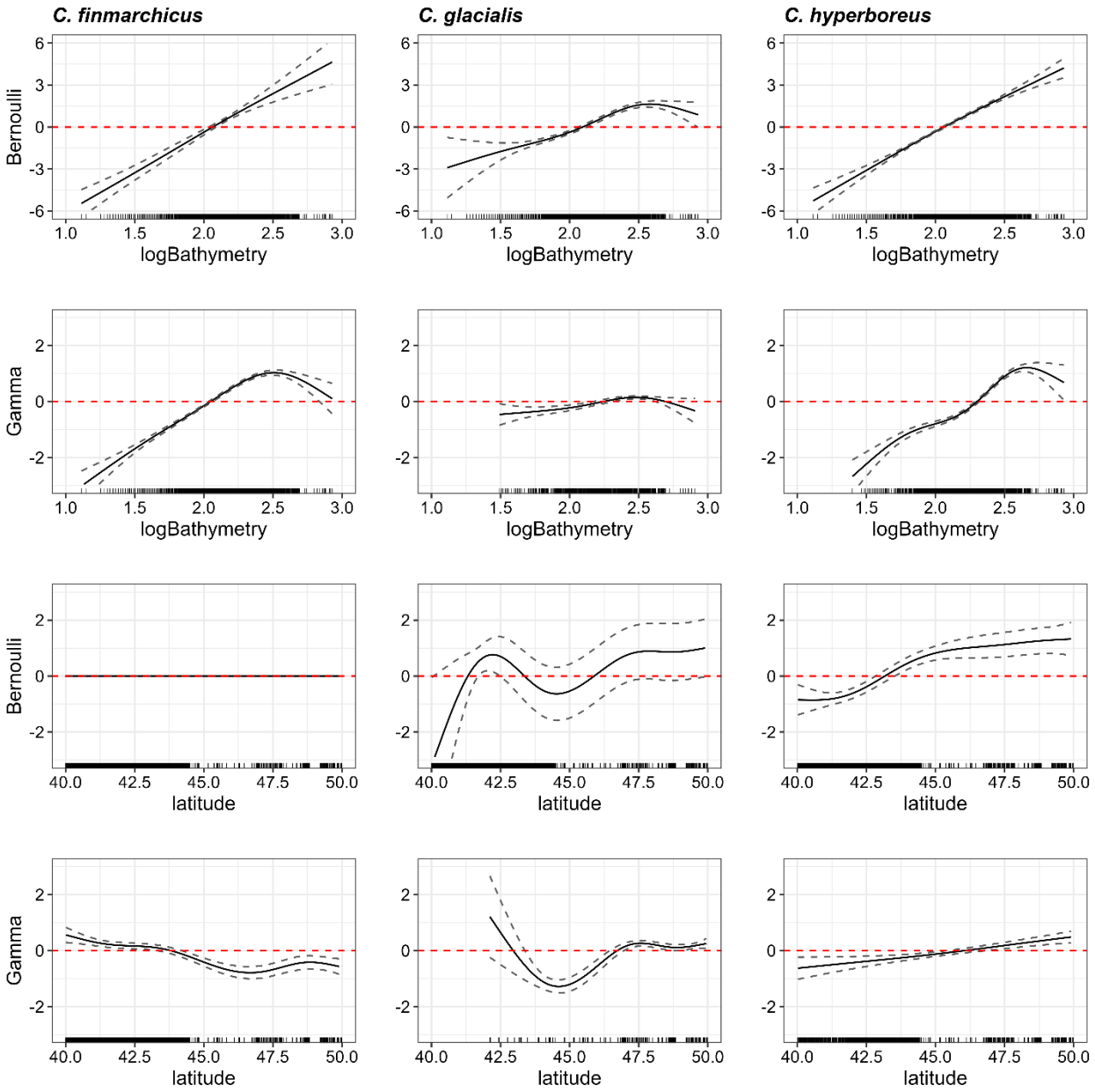

Figure 4. Partial effects for bathymetry and latitude of the Bernoulli and Gamma GAMMs for C. finmarchicus, C. glacialis, *and* C. hyperboreus *with the CanESM2_rcp8.5 simulation.*

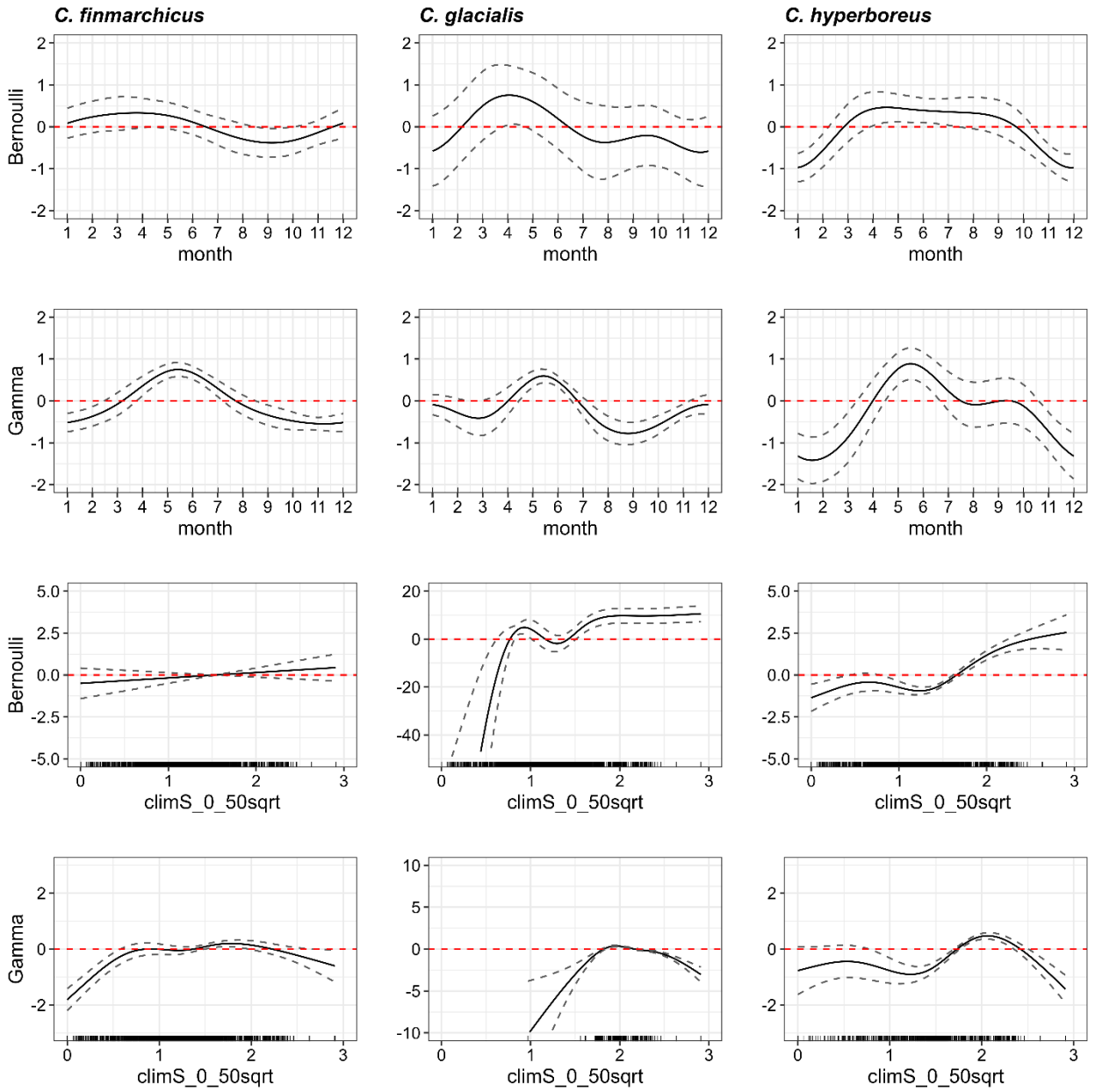

Figure 5. Partial effects for month and climS_0_50sqrt of the Bernoulli and Gamma GAMMs for C. finmarchicus, C. glacialis*, and* C. hyperboreus *with the CanESM2_rcp8.5 simulation.*

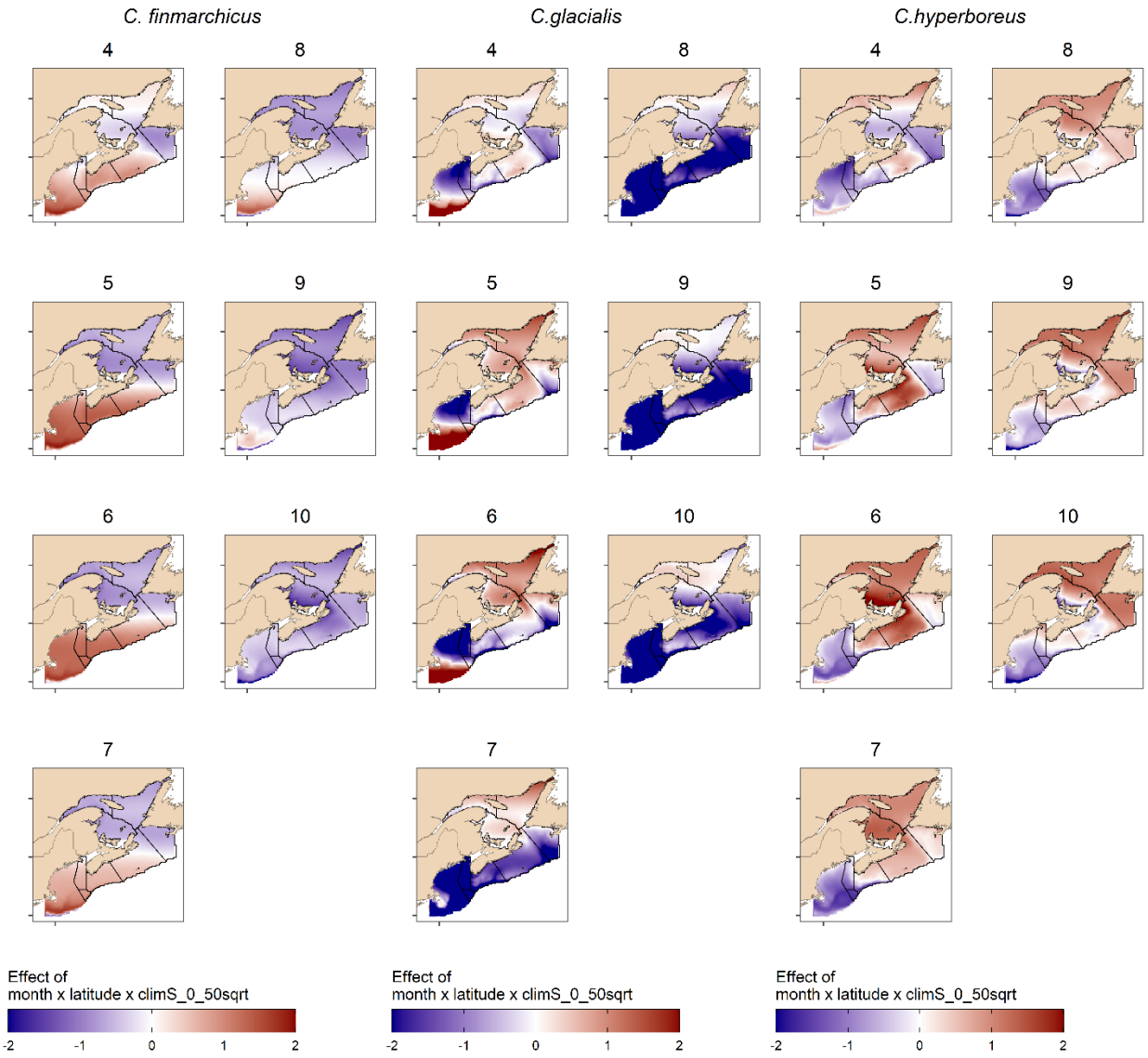

Figure 6. GAMMs :'Connectivity' term effect from April (4) to October (10) with the CanESM2_rcp8.5 regional model simulation for Calanus finmarchicus, C. glacialis *and* C. hyperboreus. *Colors represent the monthly summed effect of the connectivity term (Latitude*MONTH*ClimS_0-50sqrt) including lower level interactions and main effects. Black lines represent boundaries of regions used to report results.*

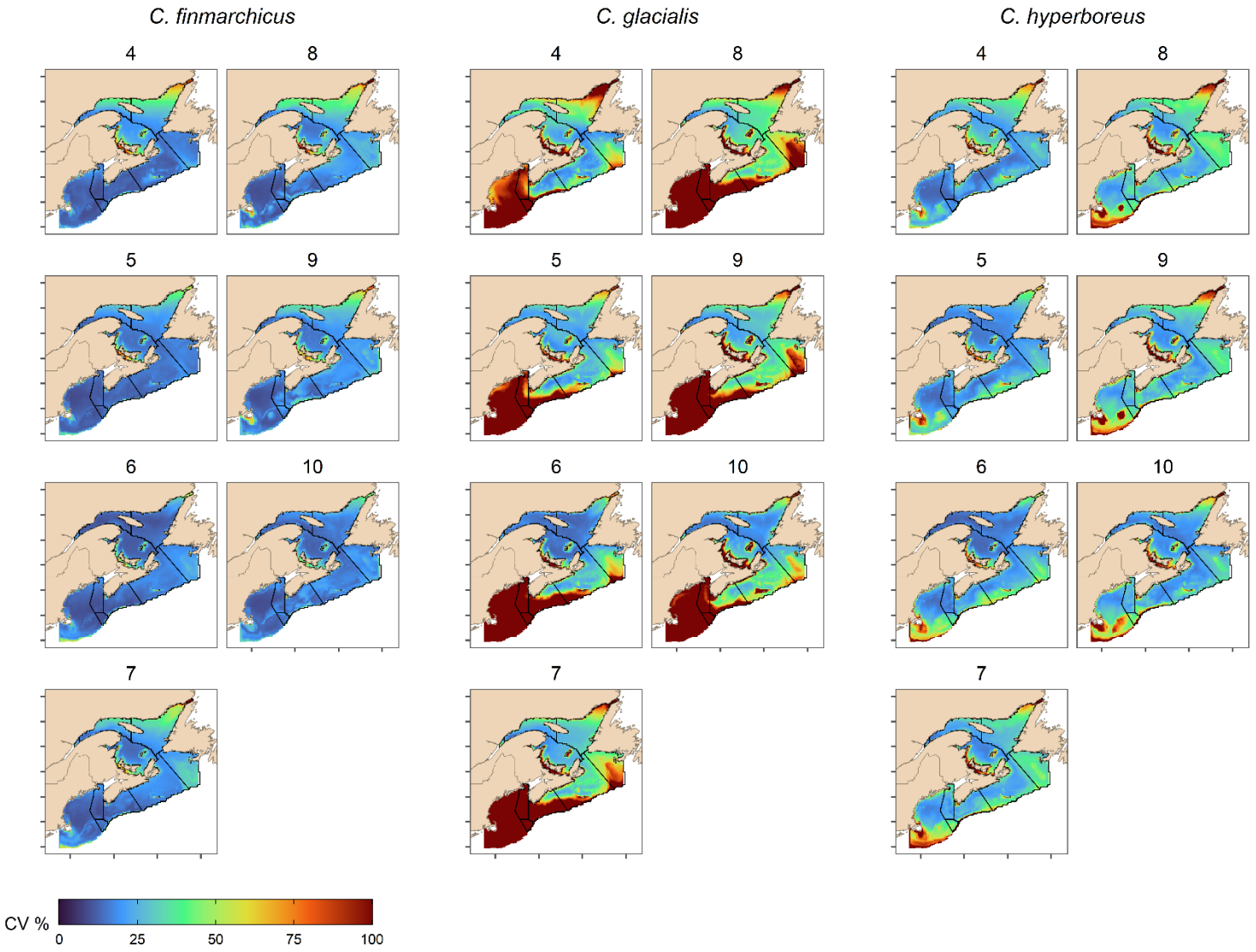

Figure 7. Coefficient of variation (CV in %) of abundance predictions for C. finmarchicus, C. glacialis *and* C. hyperboreus *during April-October 2000-2009. CVs represent the uncertainty associated with the three regional climate simulations and GAMM parameters. Black lines correspond to boundaries of regions used to report results.*

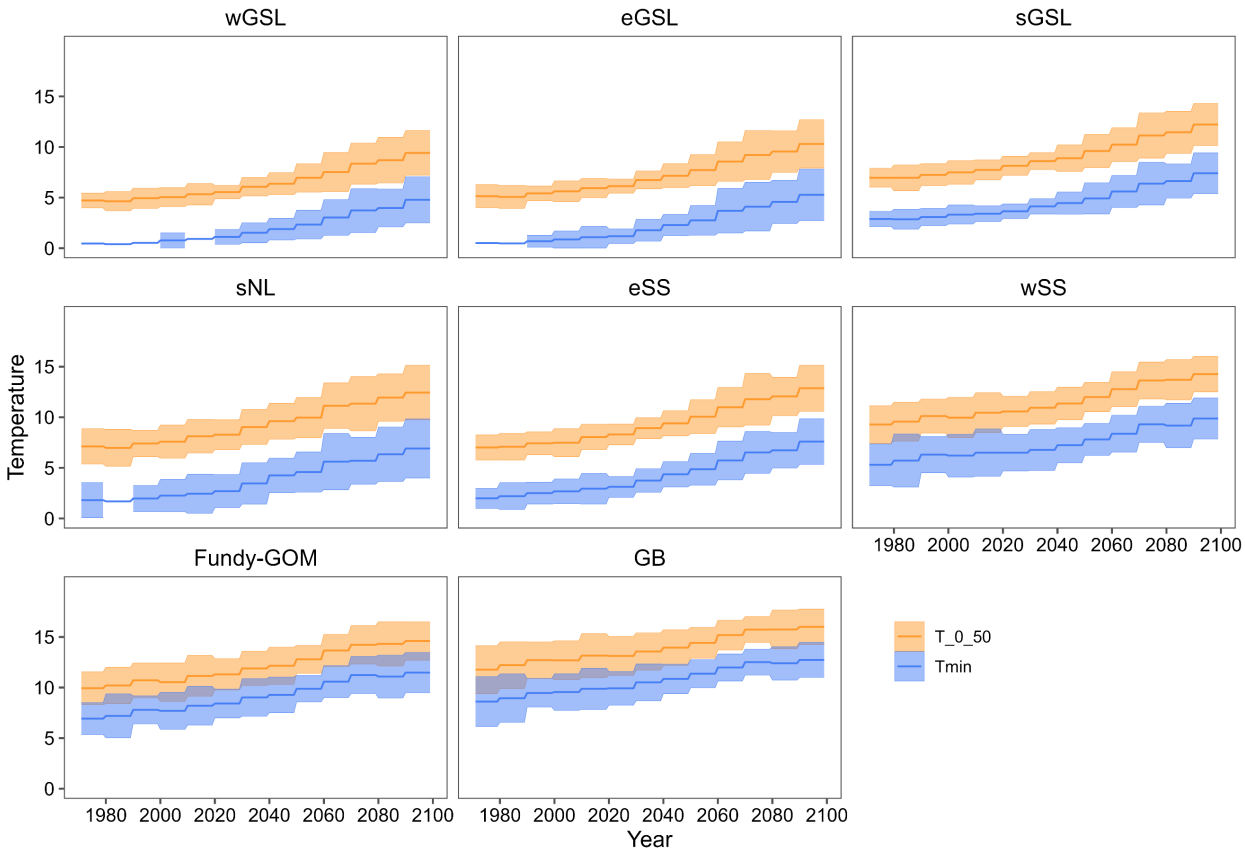

Figure 8. T_0-50 and Tmin interdecadal trends (April-October). The solid line is the mean for April-October and for the three regional climate models. The shaded area represents the uncertainty (± 1.96 SD) associated with the three regional climate simulations.*

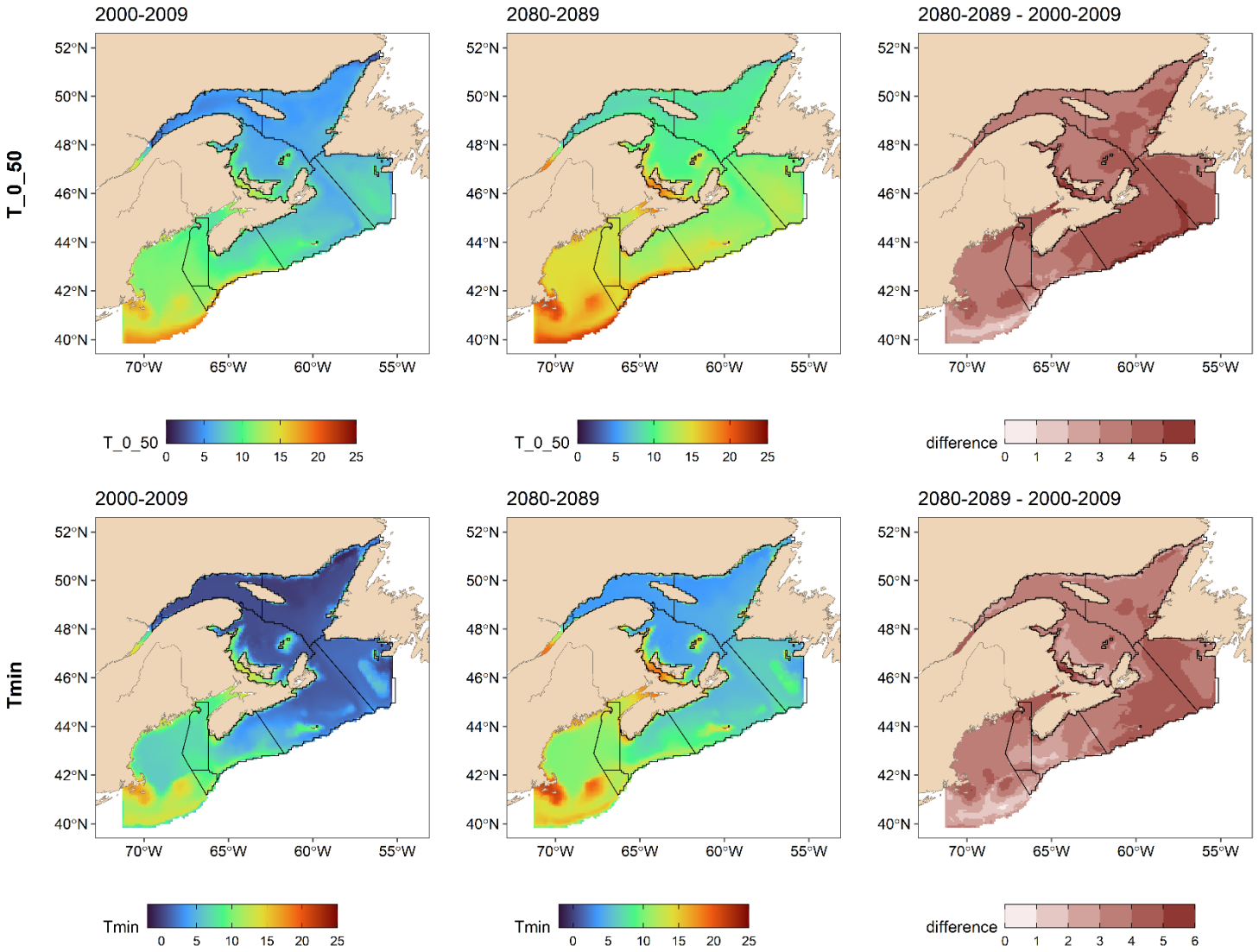

Figure 9. Climatologies of T_0-50 and Tmin. Climatologies (average of the three regional climate simulations) were calculated for April-October of 2000-2009 and 2080-2089 . Black lines represent boundaries of regions used to report results.

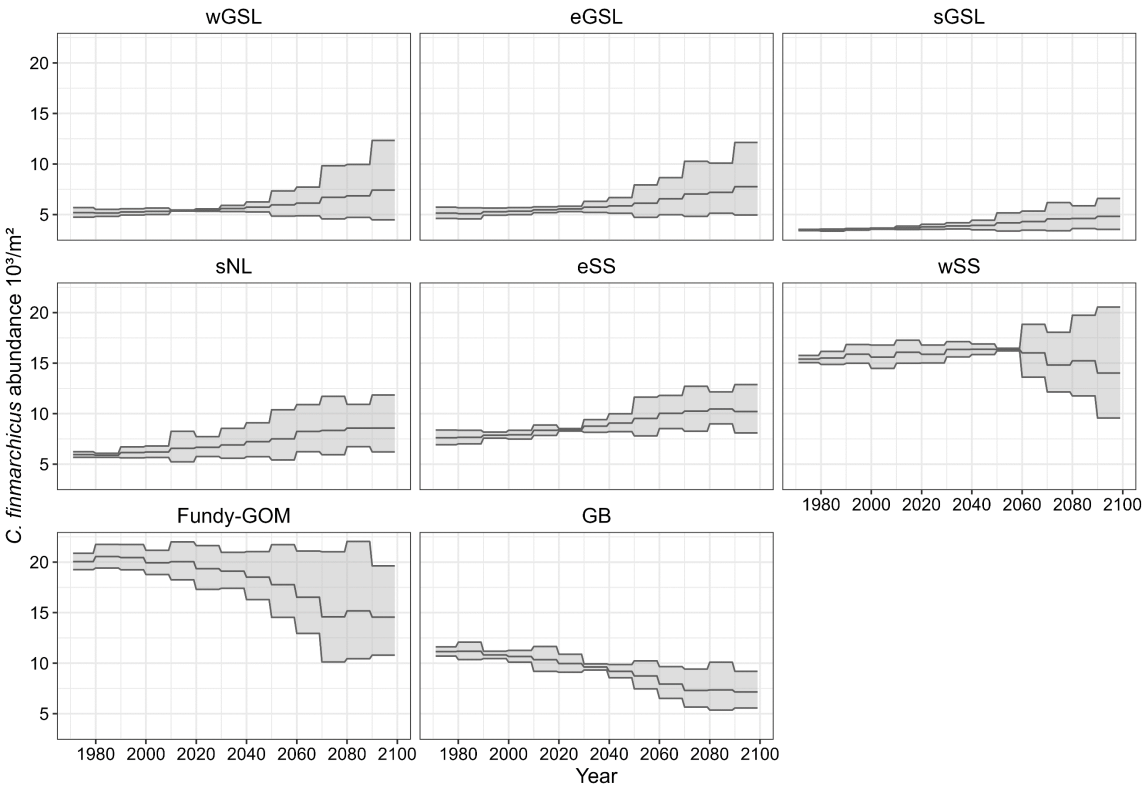

Figure 10. Trends in predicted abundance of C. finmarchicus *late stages (10³ ind m^{-2}) by decade. The black line is the mean of the three regional climate simulation scenarios for the April-October periods for each region. Grey areas represent the uncertainty around the estimated trends (± 1.96* SD).*

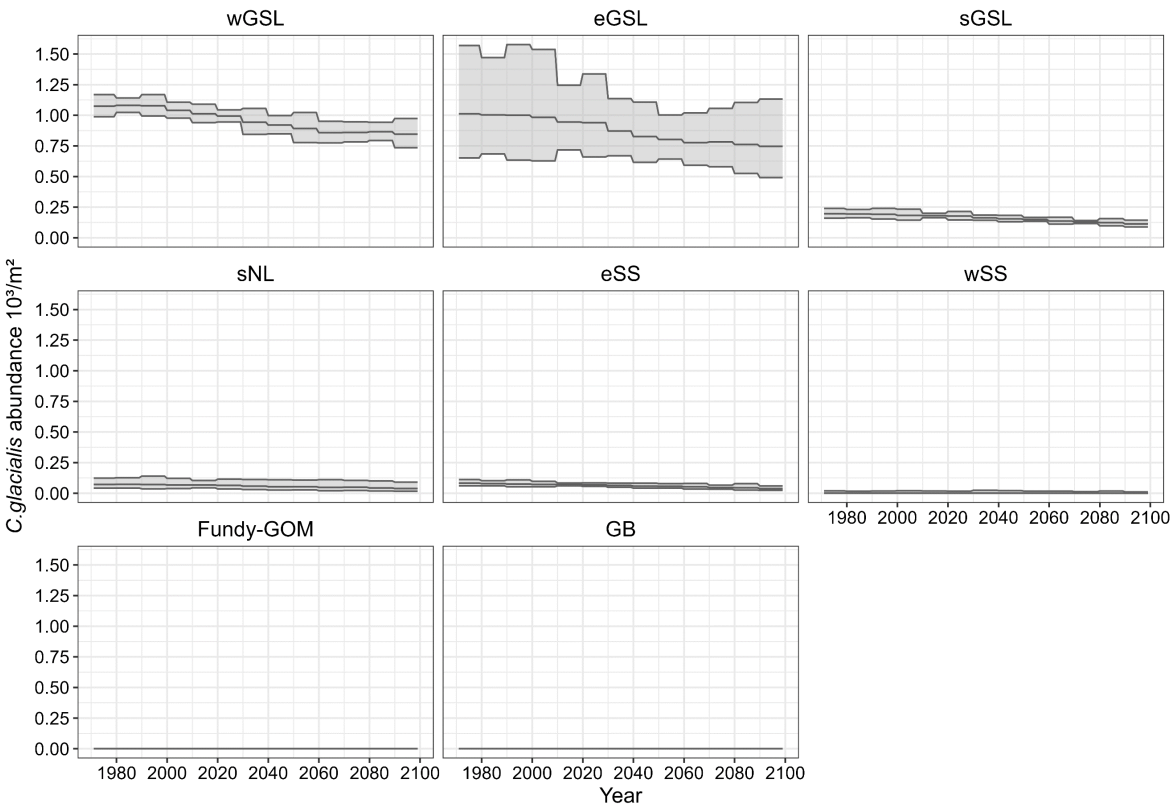

Figure 11. Trends in predicted abundance of C. glacialis *late stages (10³ ind m^{-2} by decade) for each region. The black line represents the mean of the three regional climate simulations for the April-October period. Grey areas represent the uncertainty around the estimated trends (± 1.96* SD).*

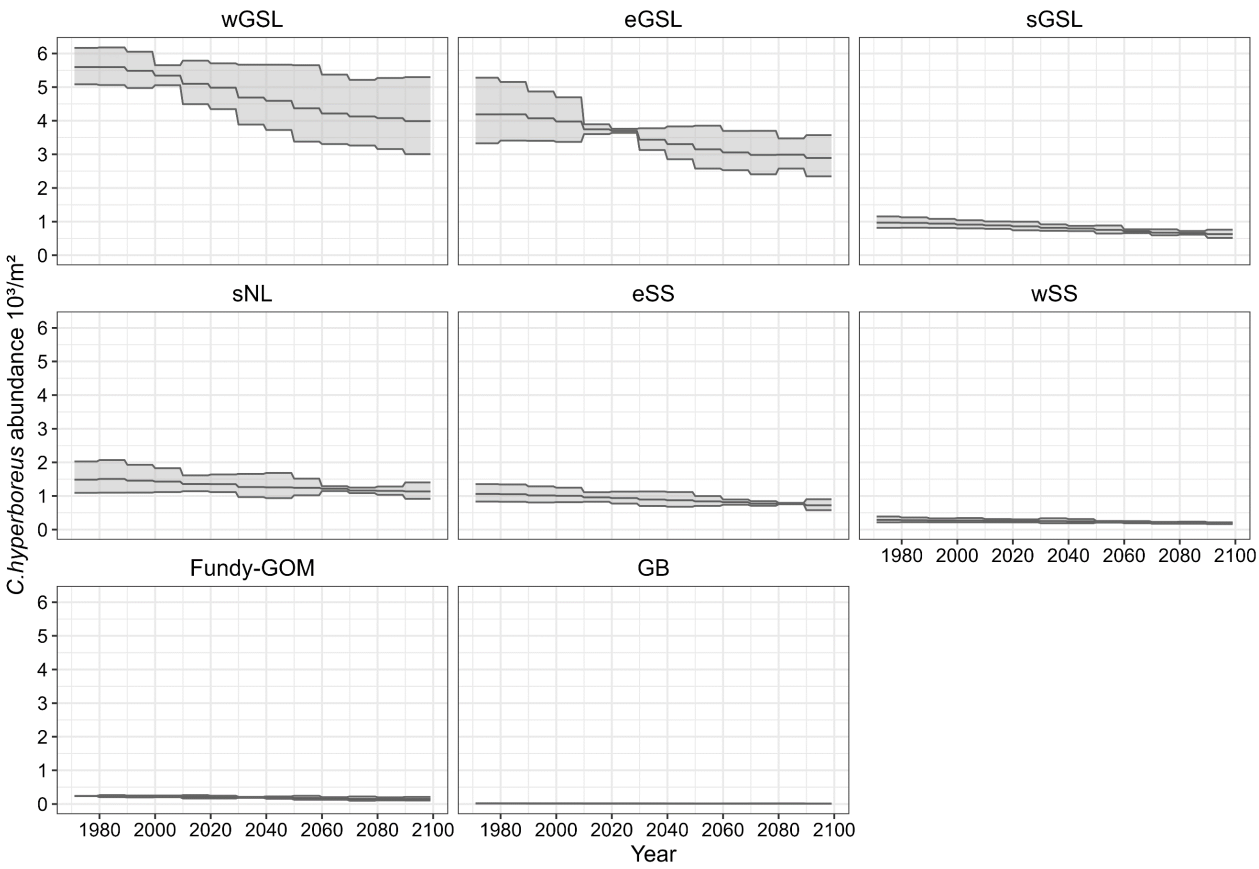

Figure 12. Trends in predicted abundance of C. hyperboreus *late stages (10^3 ind m^{-2}) by decade for each region. The black line is the mean of the three regional climate simulations for the April-October periods. Grey areas represent the uncertainty around the estimated trends (± 1.96* SD).*

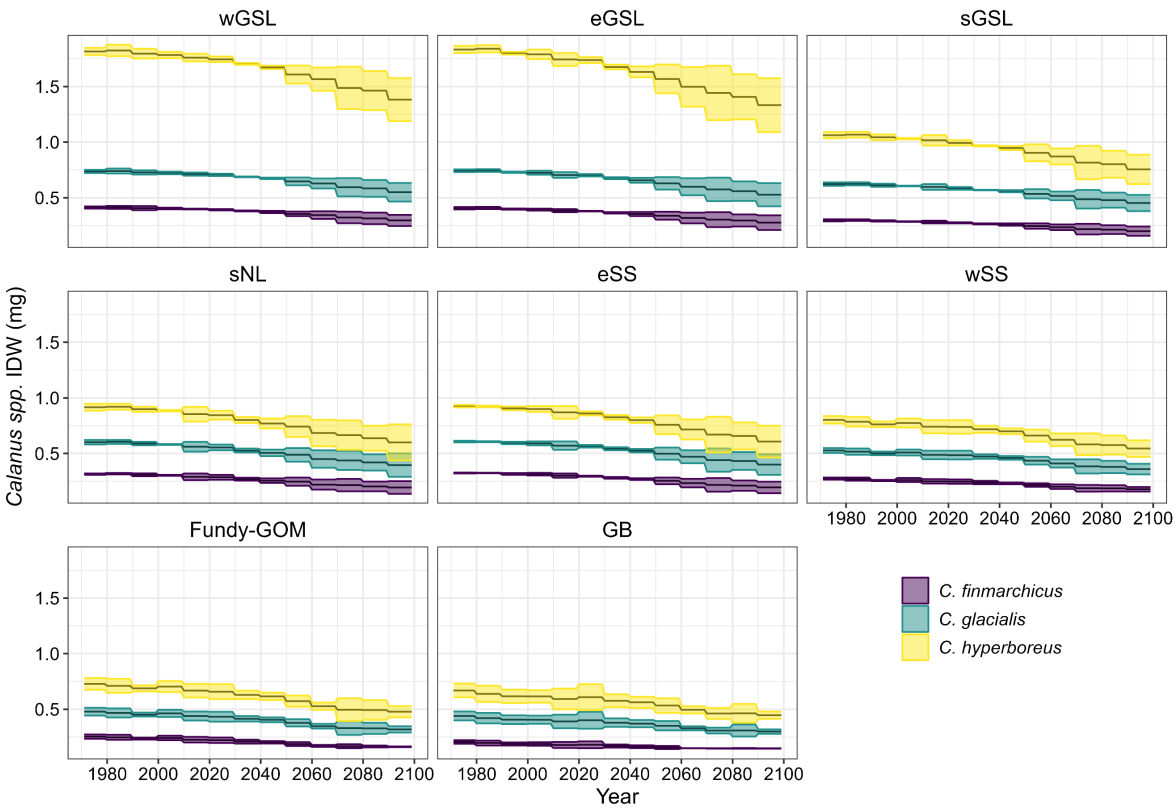

Figure 13. Calanus *CIV-CVI individual dry weight (IDW) predicted from temperature (T_0-50m) by decade and monthly stage composition, averaged for April-October by region. Black line represents the mean trend for three regional climate simulations; shaded areas correspond to the uncertainty associated with these trends (± 1.96* SD).*

Figure 14. Trends in predicted biomass of Calanus *spp. late stages (g m^{-2}). The solid line is the mean of the three regional climate simulations for the April-October and each region. Shaded areas represent the uncertainty around estimated trends (± 1.96* SD).*

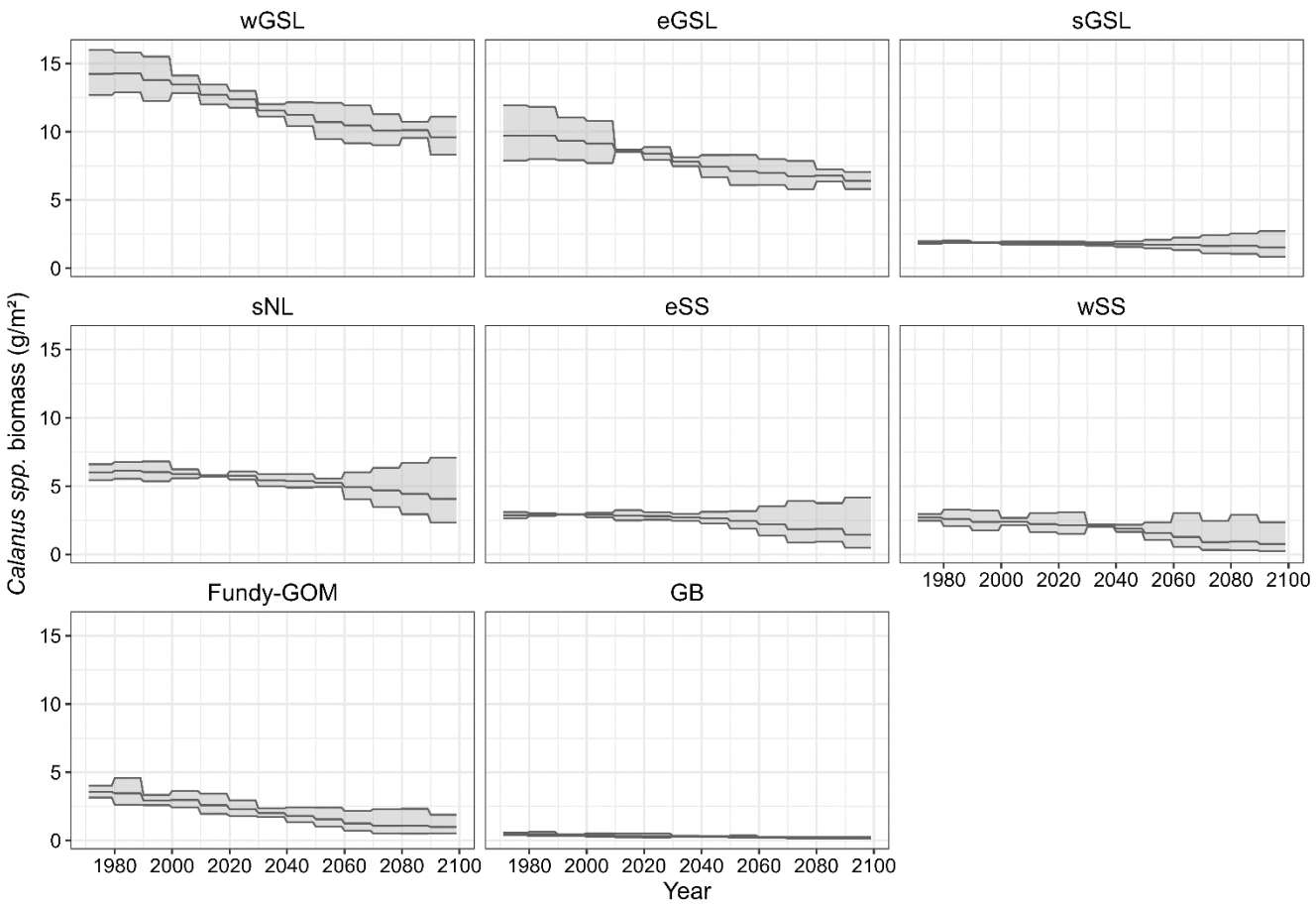

Figure 15. Trends in predicted biomass of Calanus *spp. late stages (g m^{-2}). The solid line is the mean of the three regional climate simulations for the April-October and each region. Shaded areas represent the uncertainty around estimated trends (± 1.96* SD).*

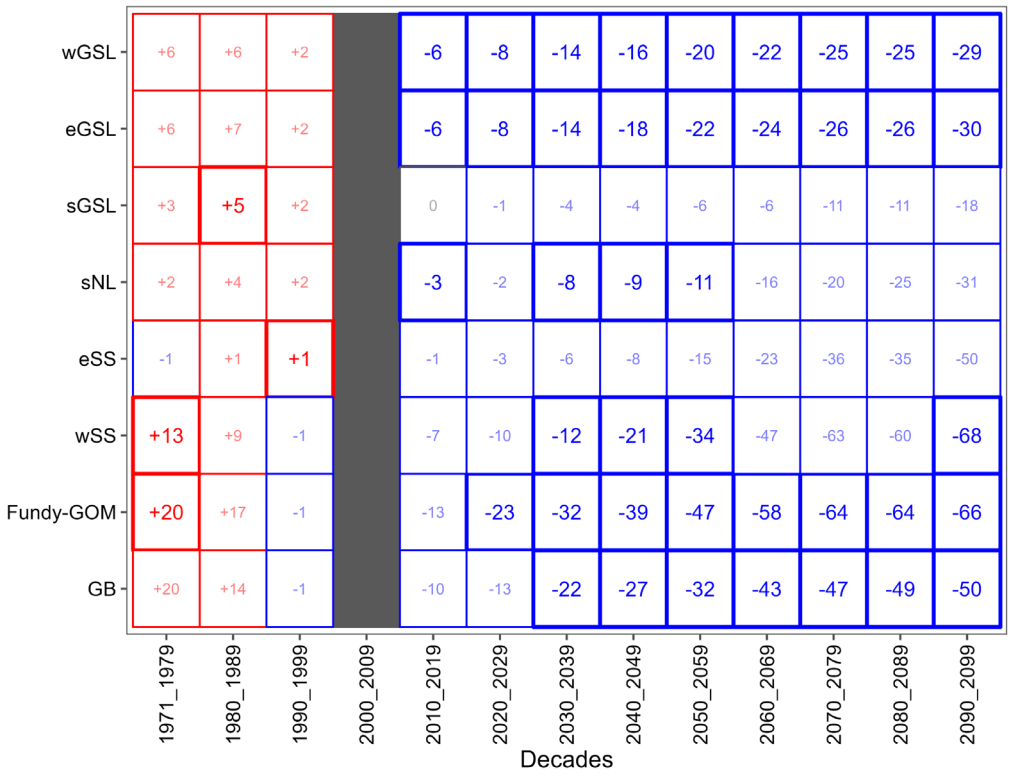

Figure 16. Interdecadal changes (%) in predicted biomass of total Calanus *species in April-October, both prior and after the 2000-2009 reference period. Red = positive difference, blue = negative difference. Bold squares and numbers = significant difference (i.e., > 1.96*SD across simulations). % change = (decade - 2000-2009) / 2000-2009*

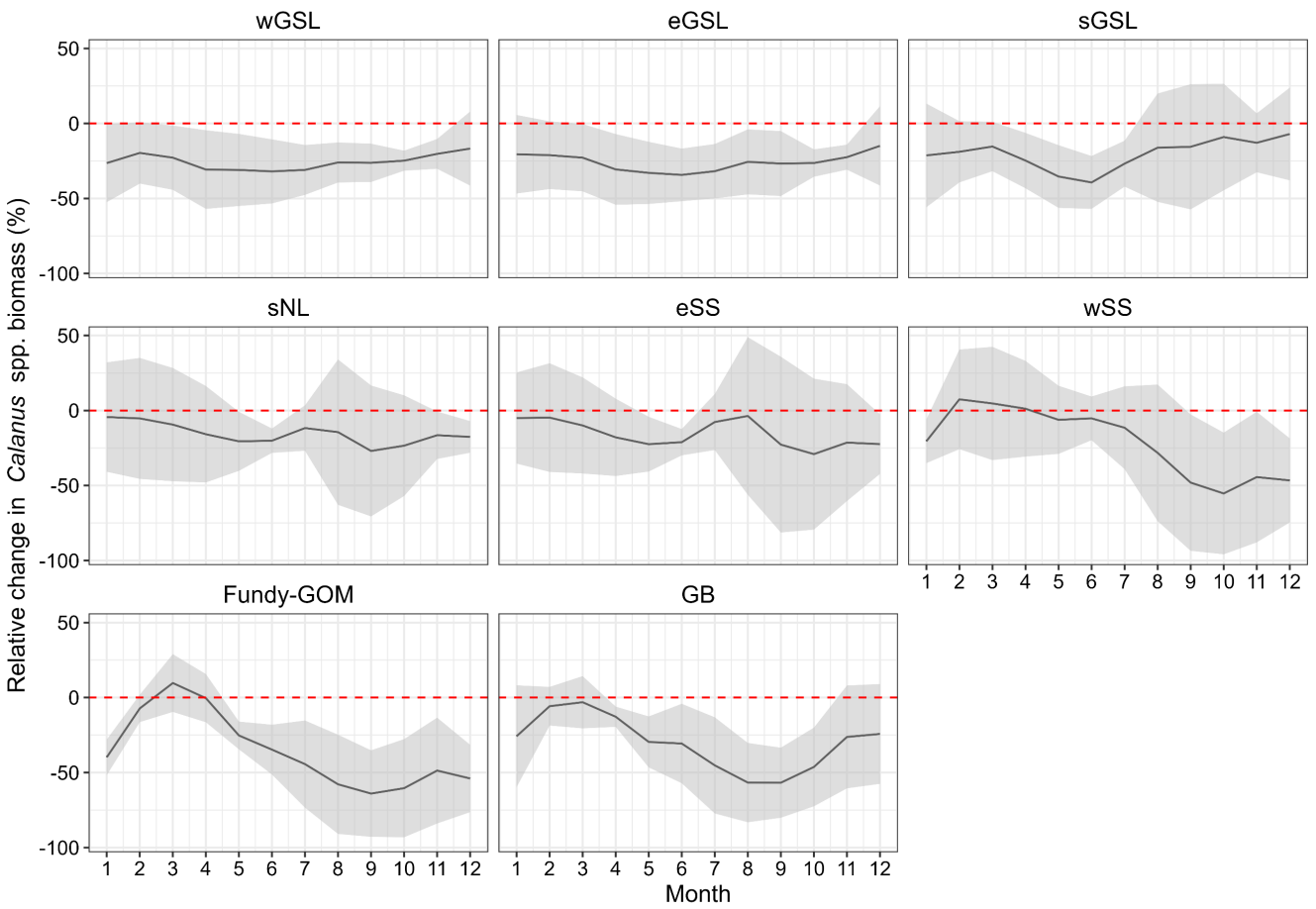

Figure 17. Mean (black line) monthly relative difference in total Calanus *predicted biomass between 2080-2089 and 2000-2009 in different regions. Shaded areas represent the uncertainty among the three regional climate simulations (± 1.96* SD).*

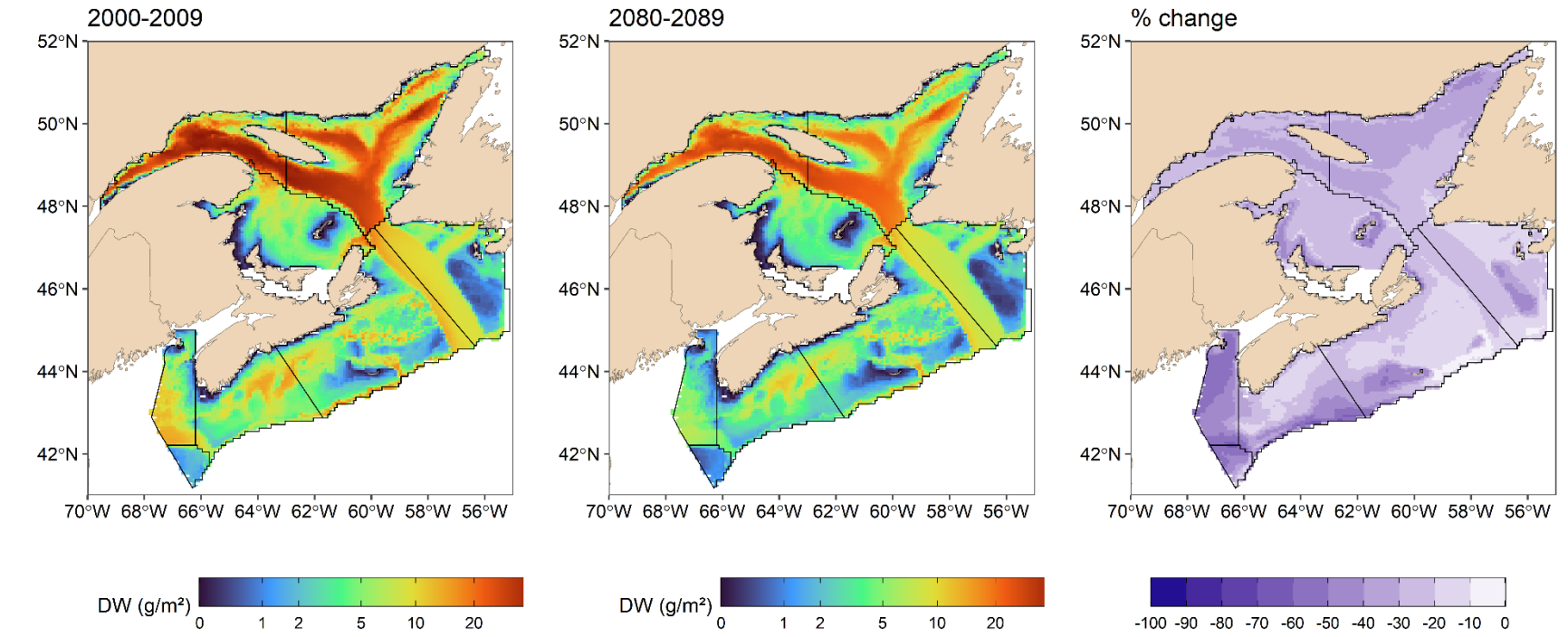

Figure 18. Change in total Calanus *predicted biomass between 2080-2089 and 2000-2009 (April-October). Black lines : boundaries of regions used to report results.*

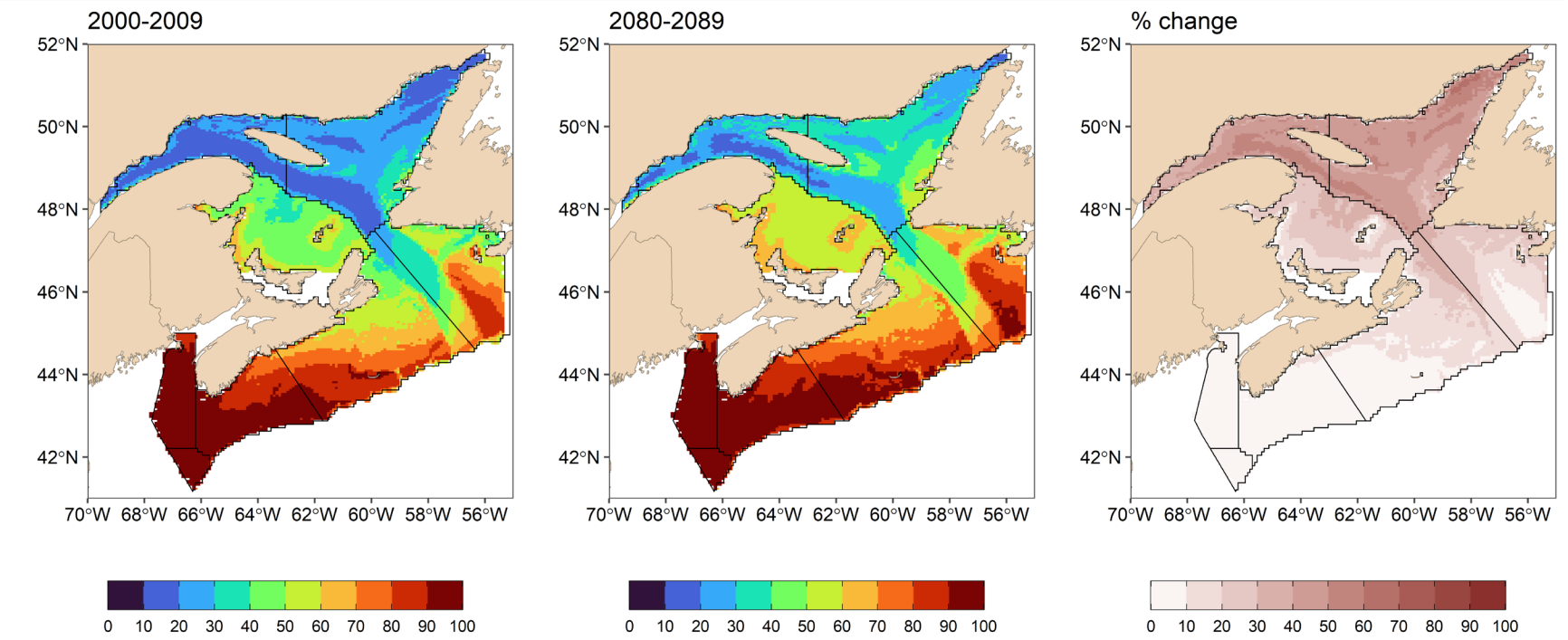

Figure 19. Contribution (%) of C. finmarchicus *to total* Calanus *predicted biomass, and % change in 2080-2089 compared to 2000-2009 (April-October). Black lines represent boundaries of regions used to report results.*

APPENDIX 1

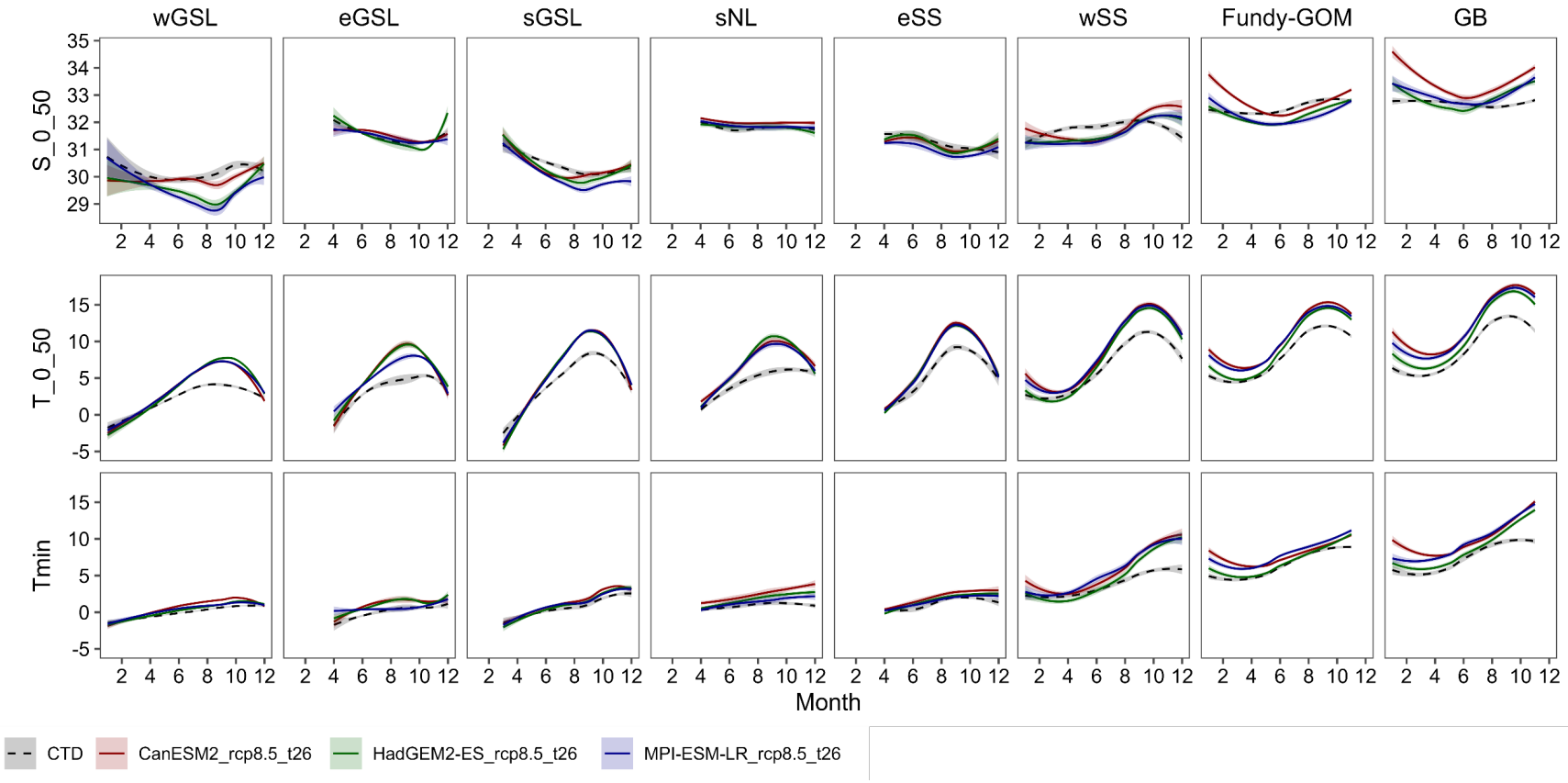

Figure A.1.1. Comparison of monthly averaged covariates during 1999-2020 extracted from CTD and from the three regional climate simulations.

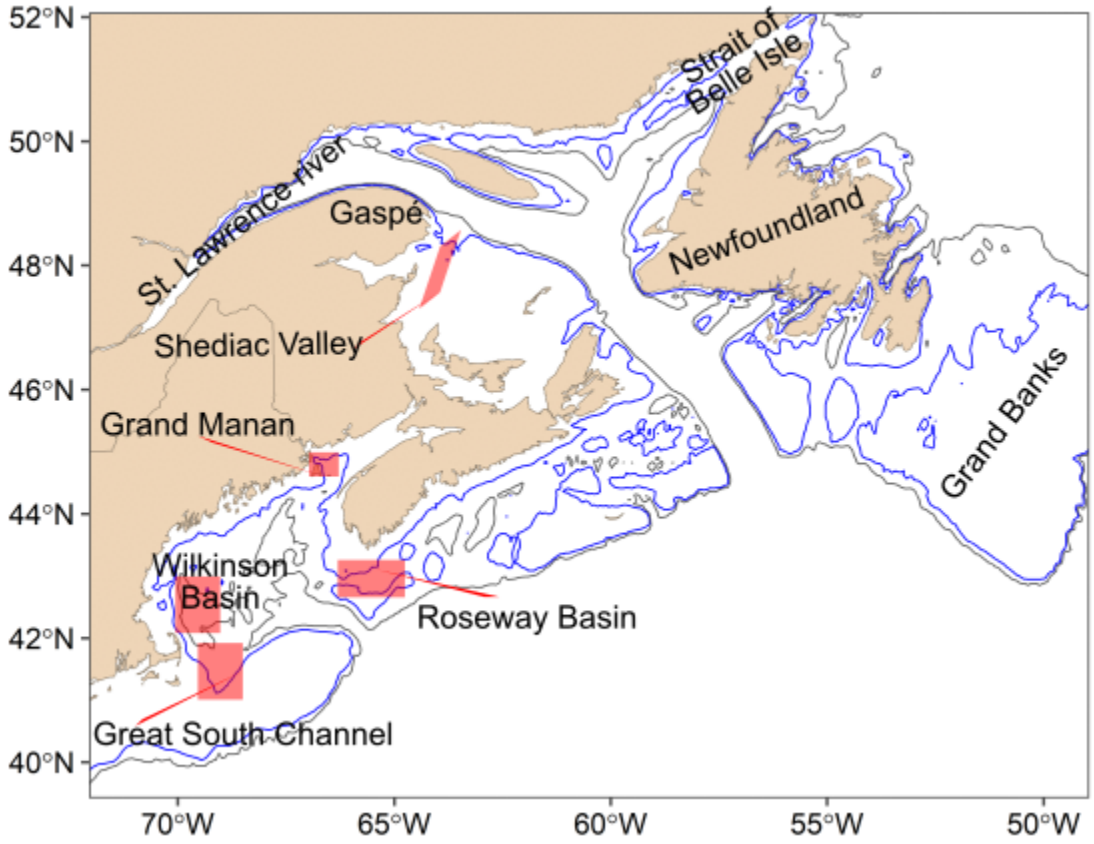

Figure A.1.2. Study area with geographic landmarks. Blue and grey lines represent the 100-m and 200-m isobaths respectively.

APPENDIX 2

Table A.2.1. Percentage of cells for which Tmin and T_0_50 were Winsorized. Percentages were calculated across approximately 15,000 spatial cells for seven months and three simulations resulting in > 300,000 values.

		% Winsorized	
Species	Decade	Tmin	T_0_50
C. finmarchicus	2000-2009	0	0
	2080-2089	0.51	1.16
C. glacialis	2000-2009	3.9	3.42
	2080-2089	7.7	14.11
C. hyperboreus	2000-2009	0.65	0.09
	2080-2089	2.9	2.36

Table A.2.2. Results for the temporal cross validation by ocean model simulation. Fit = block of years used to fit GAMMs. Valid. = block of years used to assess GAMMs performance. Bold characters = performance metric of GAMMs fitted with 100% of the data (1999-2020). Note that bold TSS values differ from table 2 because the year effect was not included in the present table for better comparison with the performance metrics calculated during cross-validation.

		Bernoulli (TSS)				Gamma (Spearman's correlation)			
Species	Model	**1999-2020 (100%)**	Fit = 2006-2020 Valid. = 1999-2005	Fit =1999-2005, 2013-2020 Valid. = 2006-2012	Fit = 1999-2012 Valid. = 2013-2020	**1999-2020 (100%)**	Fit = 2006-2020 Valid. = 1999-2005	Fit =1999-2005, 2013-2020 Valid. = 2006-2012	Fit = 1999-2012 Valid. = 2013-2020
C. finmarchicus	CanESM2_rcp8.5	**0.58**	0.48	0.60	0.55	**0.70**	0.71	0.67	0.68
	HadGEM2-ES_rcp8.5	**0.59**	0.51	0.57	0.55	**0.70**	0.71	0.66	0.67
	MPI-ESM-LR_rcp8.5	**0.58**	0.50	0.61	0.57	**0.70**	0.71	0.66	0.67
C. glacialis	CanESM2_rcp8.5	**0.85**	0.85	0.88	0.79	**0.51**	0.38	0.51	0.63
	HadGEM2-ES_rcp8.5	**0.85**	0.85	0.89	0.79	**0.59**	0.44	0.42	0.61
	MPI-ESM-LR_rcp8.5	**0.85**	0.85	0.89	0.80	**0.53**	0.39	0.58	0.59
C. hyperboreus	CanESM2_rcp8.5	**0.65**	0.59	0.65	0.73	**0.73**	0.67	0.74	0.78
	HadGEM2-ES_rcp8.5	**0.64**	0.60	0.65	0.71	**0.72**	0.66	0.73	0.77
	MPI-ESM-LR_rcp8.5	**0.63**	0.60	0.65	0.73	**0.73**	0.66	0.74	0.78

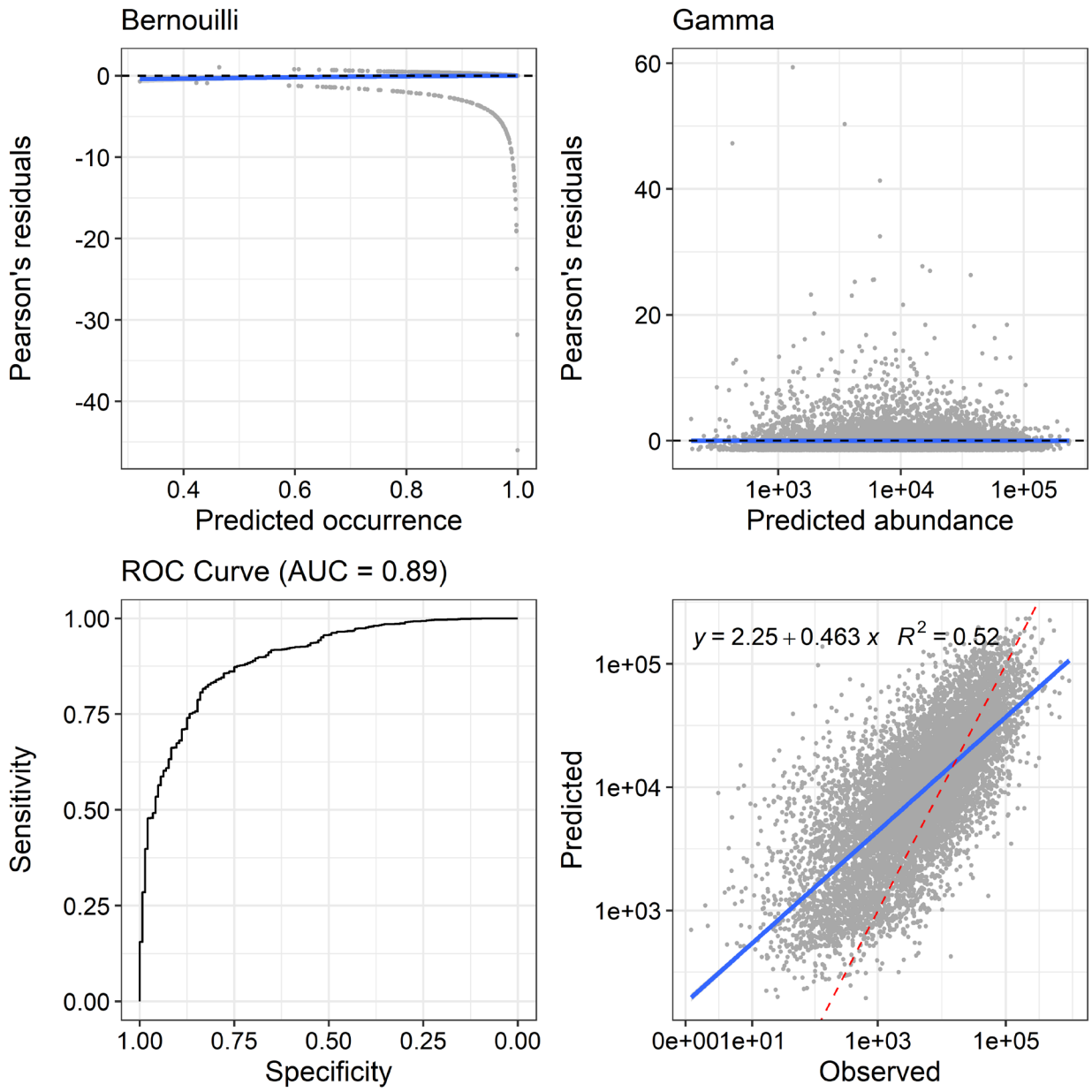

Figure A.2.1. Validation of the Bernoulli (left) and Gamma GAMMs (right) for C. finmarchicus *using the CanESM2_rcp8.5 simulation. Homogeneity was verified (upper panels), with the expectation that the smoother on the Pearson's residuals against the predictions (blue) should near 0 (black dashed line). The accuracy of predictions was verified with the ROC curve for the Bernoulli (left, see also Table 2 for TSS) and a linear relationship between abundance predictions and observations in the case of the Gamma GAMMs (blue line) The red dash line indicates perfect predictions (slope =1, intercept=0).*

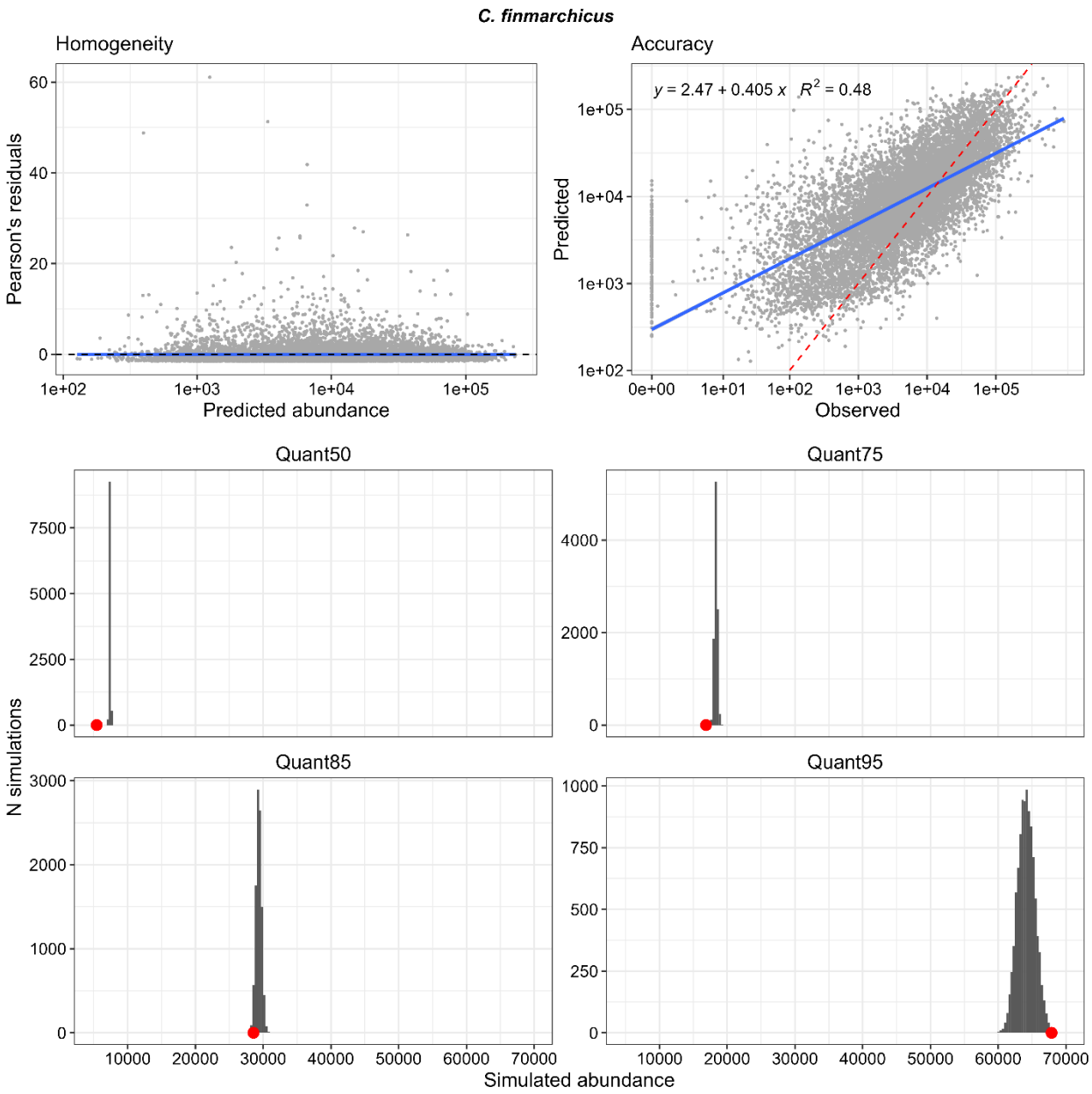

Figure A.2.2. Validation of the ZAG GAMM (π x μ) for C. finmarchicus *using the CanESM2_rcp8.5 scenario. Homogeneity and accuracy were verified (upper panel); see Figure A.2.1 for details on how this was done. The ZAG distribution of parameter simulations (grey histograms) was verified against the observations for each of the 50,75,85 and 95 quantiles (red circles) (four bottom panels).*

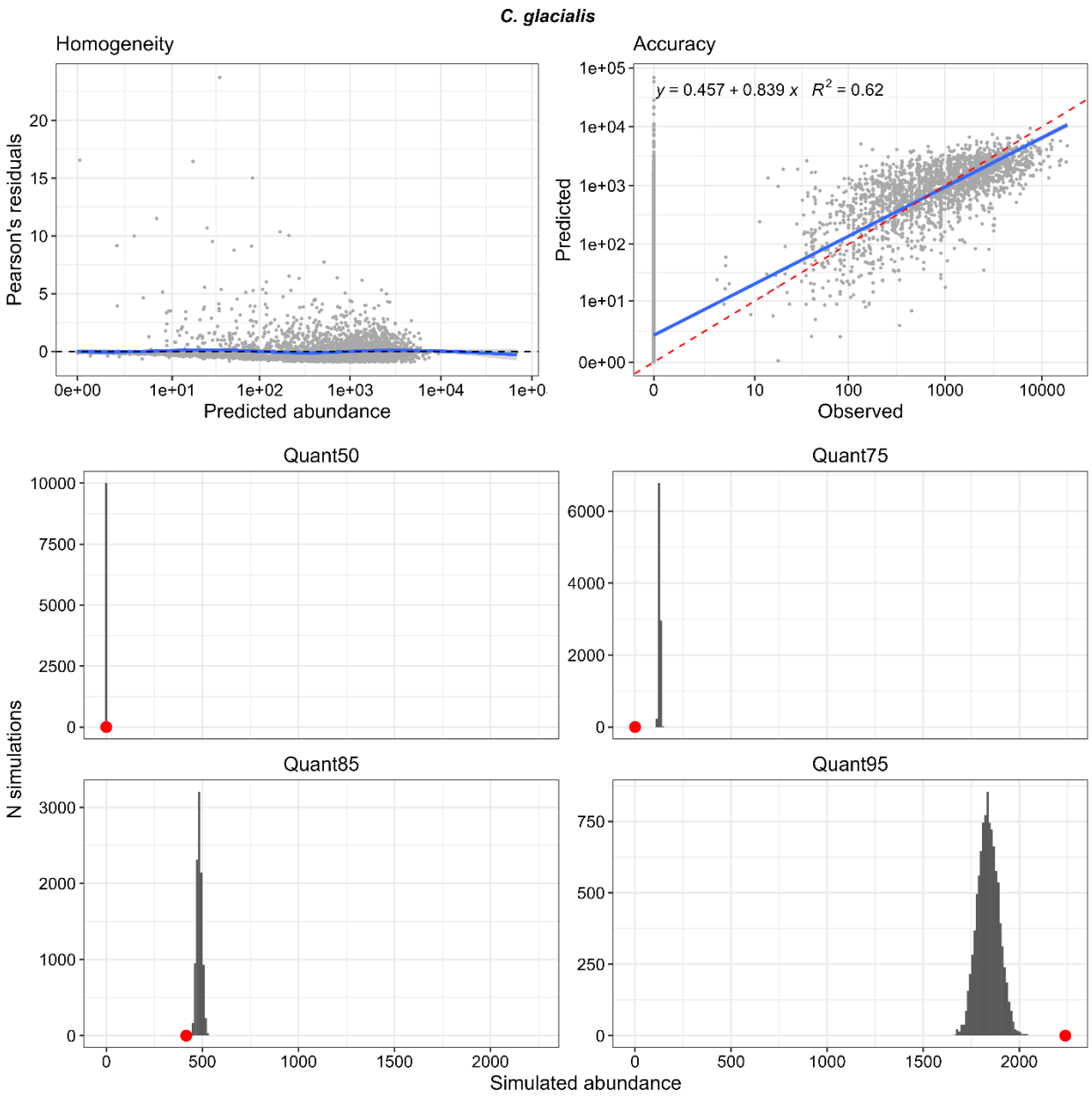

Figure A.2.3. Validation of the ZAG GAMMs (π x μ) for C. glacialis *using the CanESM2_rcp8.5 scenario. Homogeneity and accuracy were verified (upper panel; see Figure A.2.1 for details). The ZAG distribution of parameter simulations (grey histograms) was verified against the observations for each of the 50,75,85 and 95 quantiles (red circles) (four bottom panels).*

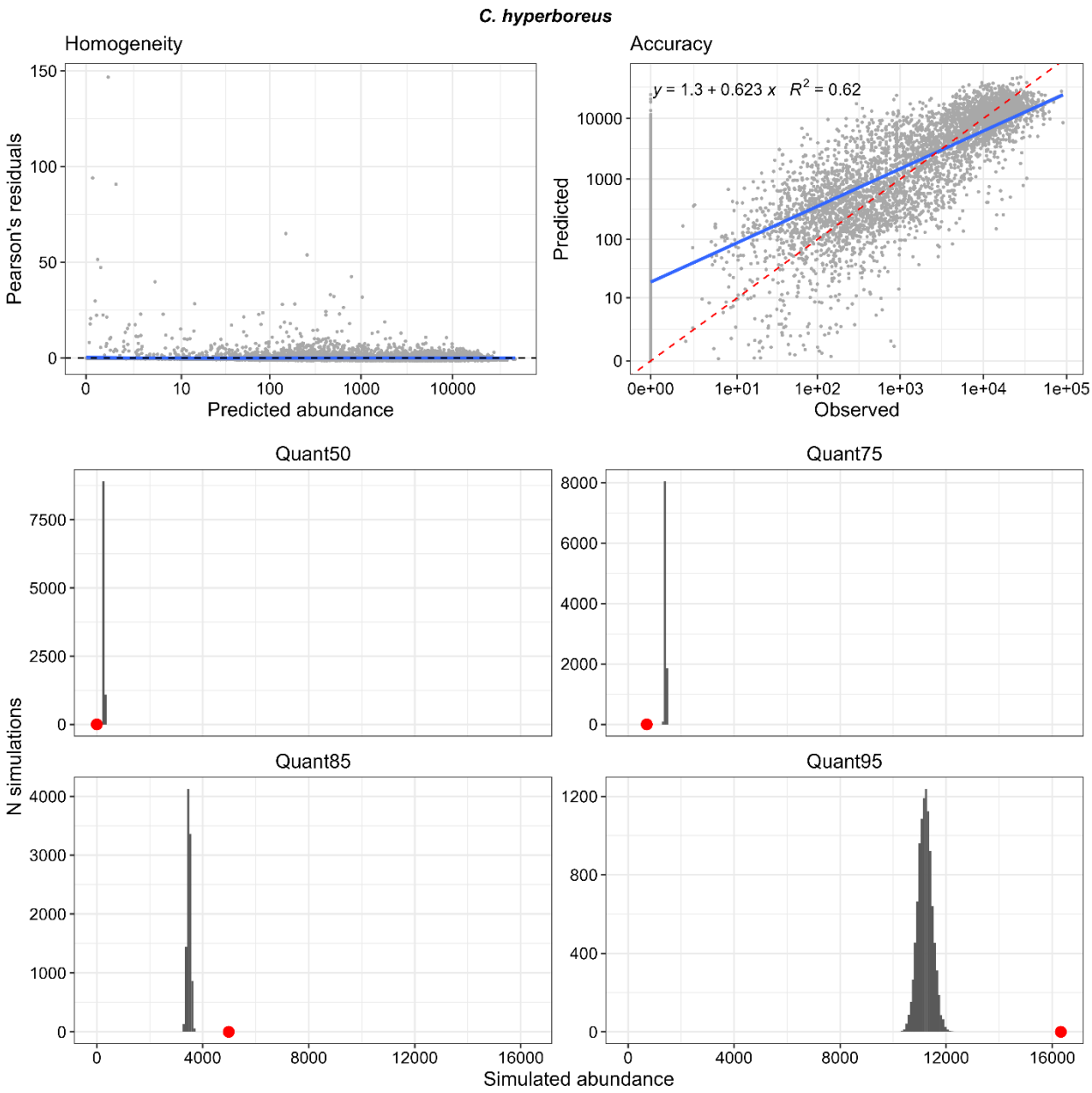

Figure A.2.4. Validation of the ZAG GAMMs (π x μ) for C. hyperboreus *using the CanESM2_rcp8.5 scenario. Homogeneity and accuracy were verified (upper panels); see Figure A.2.1 for details. The ZAG distribution of parameter simulations (grey histograms) was verified against the observations for each of the 50,75,85 and 95 quantiles (red circles) (four bottom panels).*

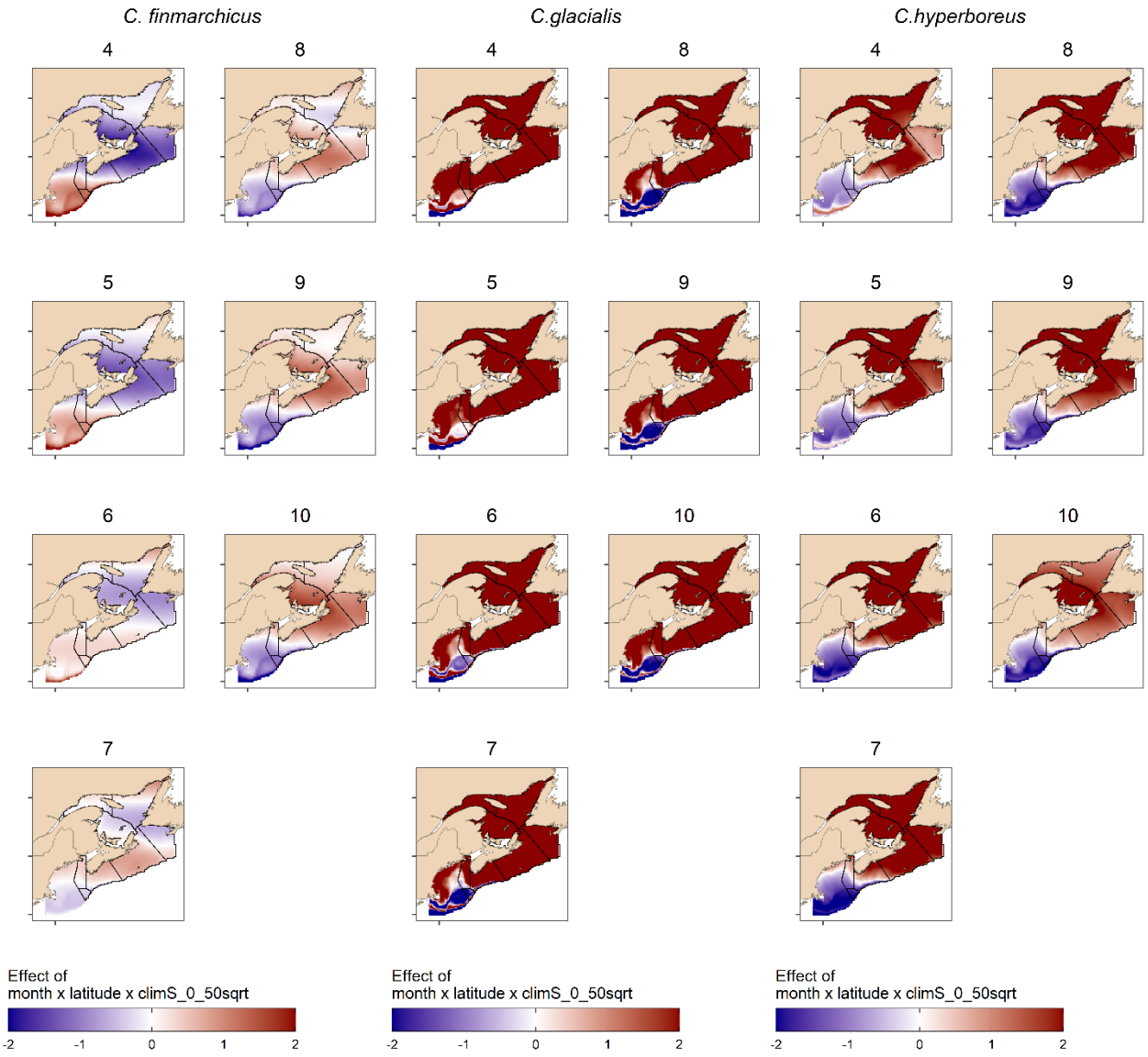

Figure A.2.5. GAMM :'Connectivity' term effect with the CanESM2_rcp8.5 regional model simulation for Calanus finmarchicus, C. glacialis *and* C. hyperboreus. *Effect include Latitude*MONTH*ClimS_0-50m. Black lines represent boundaries of regions used to report results.*

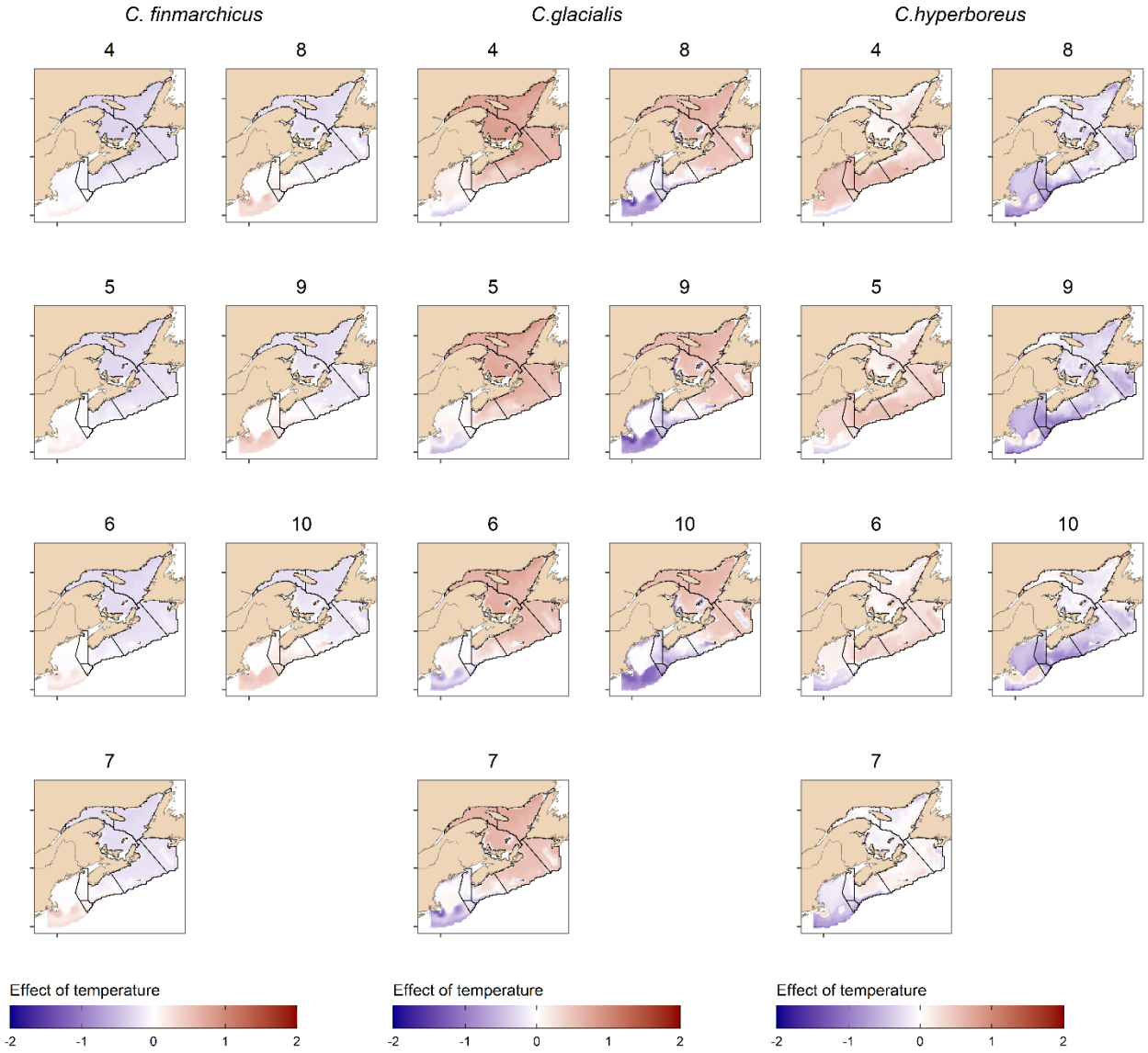

Figure A.2.6. Bernoulli GAMM: Combined effect of T_0-50 and Tmin on the presence/absence of Calanus finmarchicus*,* C. glacialis *and* C. hyperboreus*. Black lines represent boundaries of regions used to report results.*

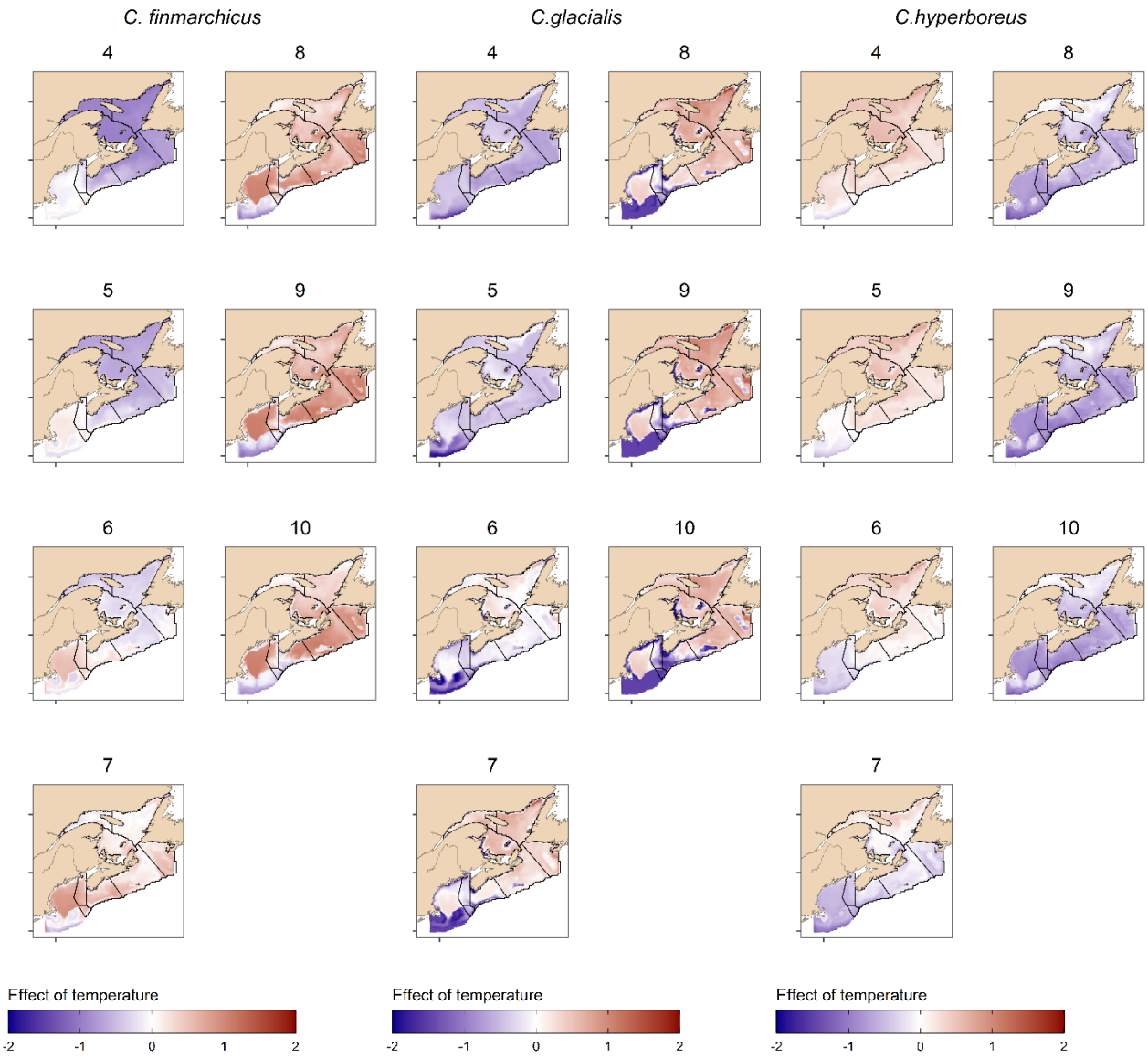

Figure A.2.7. Gamma GAMM: Combined effect of T_0-50 and Tmin on the abundance of Calanus finmarchicus, C. glacialis *and* C. hyperboreus *1999-2020. Black lines represent boundaries of regions used to report results.*

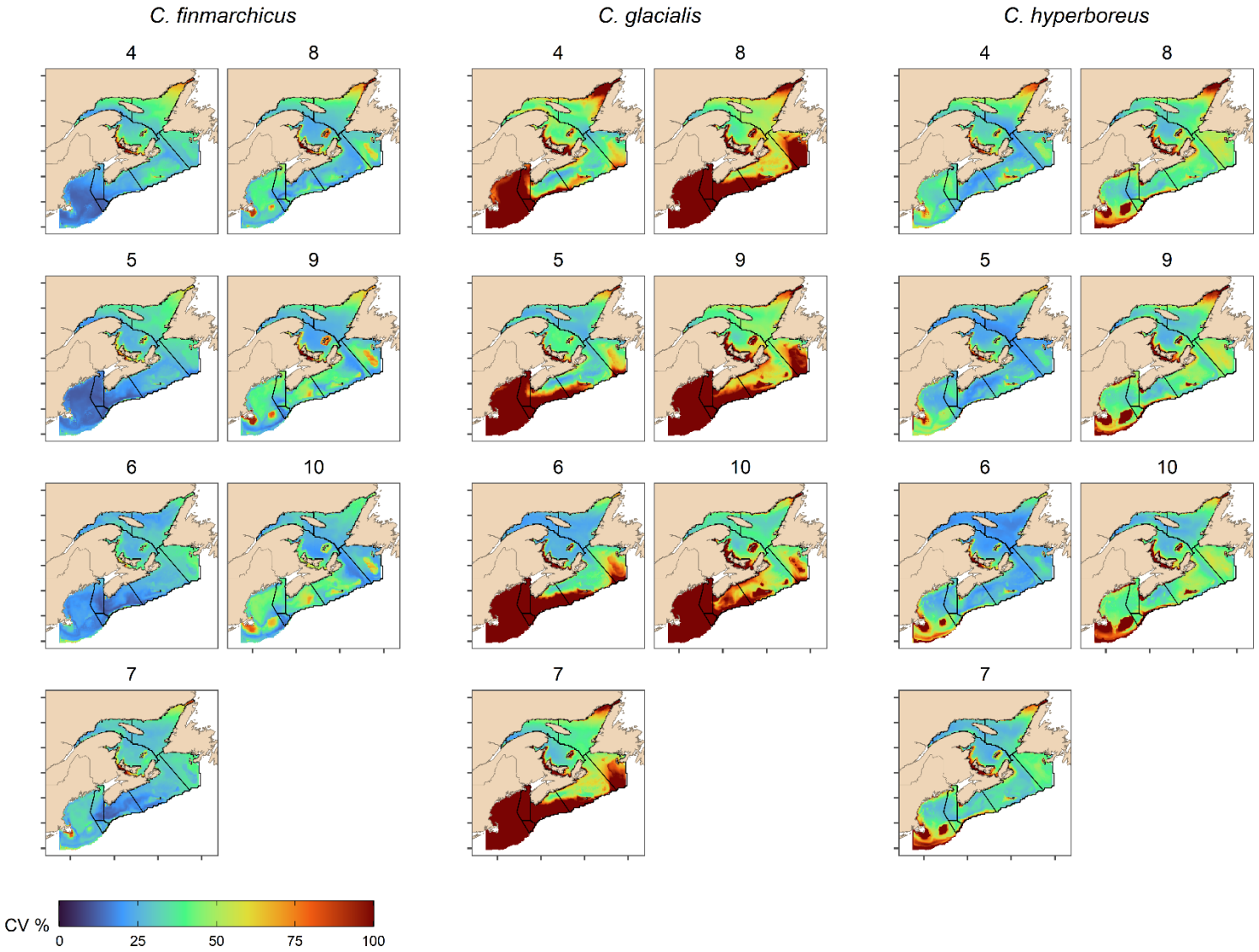

Figure A.2.8. Coefficient of variation (CV in %) of mean abundance predictions of C. finmarchicus, C. glacialis *and* C. hyperboreus *during April-October 2080-2089. The CV represents the uncertainty associated with the three regional climate simulations and GAMM parameters. Black lines represent boundaries of regions used to report results.*